nature medicine

LETTERS

https://doi.org/10.1038/s41591-019-0504-5

Healthspan and lifespan extension by fecal microbiota transplantation into progeroid mice

Clea Bárcena[1], Rafael Valdés-Mas[1], Pablo Mayoral[1], Cecilia Garabaya[1], Sylvère Durand[2,3,4,5], Francisco Rodríguez[1], María Teresa Fernández-García[6], Nuria Salazar[7,8], Alicja M. Nogacka[7,8], Nuria Garatachea[9,10], Noélie Bossut[2,3,4,5], Fanny Aprahamian[2,3,4,5], Alejandro Lucia[11,12], Guido Kroemer[2,3,4,5,13,14,15], José M. P. Freije[1,16], Pedro M. Quirós[1,16*] and Carlos López-Otín[1,16*]

The gut microbiome is emerging as a key regulator of several metabolic, immune and neuroendocrine pathways[1,2]. Gut microbiome deregulation has been implicated in major conditions such as obesity, type 2 diabetes, cardiovascular disease, non-alcoholic fatty acid liver disease and cancer[3–6], but its precise role in aging remains to be elucidated. Here, we find that two different mouse models of progeria are characterized by intestinal dysbiosis with alterations that include an increase in the abundance of Proteobacteria and Cyanobacteria, and a decrease in the abundance of Verrucomicrobia. Consistent with these findings, we found that human progeria patients also display intestinal dysbiosis and that long-lived humans (that is, centenarians) exhibit a substantial increase in Verrucomicrobia and a reduction in Proteobacteria. Fecal microbiota transplantation from wild-type mice enhanced healthspan and lifespan in both progeroid mouse models, and transplantation with the verrucomicrobia *Akkermansia muciniphila* was sufficient to exert beneficial effects. Moreover, metabolomic analysis of ileal content points to the restoration of secondary bile acids as a possible mechanism for the beneficial effects of reestablishing a healthy microbiome. Our results demonstrate that correction of the accelerated aging-associated intestinal dysbiosis is beneficial, suggesting the existence of a link between aging and the gut microbiota that provides a rationale for microbiome-based interventions against age-related diseases.

Traditionally seen as detrimental, the pathophysiological implications of the microbiota have expanded considerably in recent years. It is now known that the microbiota has essential metabolic and immunological functions that are conserved from worms[7] to humans[1,2]. In mammals, the gut microbiota is involved in food processing, activation of satiety pathways, protection against pathogens and production of metabolites including vitamins, short-chain fatty acids and secondary bile acids[8–10]. The gut microbiota also signals to distant organs, contributing to the maintenance of host physiology[11]. Intestinal microbiota alterations are associated with major conditions like obesity, type 2 diabetes, cardiovascular disease, non-alcoholic fatty acid liver disease, cancer and the response to antineoplastic therapy[3–6].

Although some works have explored the microbiome profile of long-lived humans[12,13], no alterations have been described in accelerated aging syndromes. In this work, we study the gut microbiome of two mouse models of Hutchinson–Gilford progeria syndrome (HGPS), patients with HGPS[14] and Nestor–Guillermo progeria syndrome (NGPS)[15], as well as human centenarians and their controls. We found intestinal dysbiosis in both mouse models and progeria patients. In turn, the microbiota of centenarians is characterized by the presence of both pathological and health-associated bacterial genera. We show that fecal microbiota transplantation (FMT) from wild-type (WT) donors to progeroid recipients attenuates the accelerated-aging phenotype and increases survival, whereas FMT from progeroid donors to WT recipients induces metabolic alterations. Analysis of centenarians and progeria mouse models points to a beneficial role for the genus *Akkermansia*, as oral gavage of *Akkermansia muciniphila* extends the lifespan of progeroid mice.

To explore the relevance of the microbiome in progeria, we first studied the gut metagenome profile of the $Lmna^{G609G/G609G}$ mouse model of HGPS[16], by comparing WT and $Lmna^{G609G/G609G}$ mice at three different ages: 1 month (WT 1mo and $Lmna^{G609G/G609G}$ 1mo), 4 months (when $Lmna^{G609G/G609G}$ mice exhibit a progeroid phenotype; WT 4mo and $Lmna^{G609G/G609G}$ 4mo) and 22 months (for WT mice only; WT 22mo; Extended Data Fig. 1a). To assess how progeria affects the gut microbial community structure, we studied the alpha- and beta-diversity associated with each genotype and compared the microbial diversity within and between communities. Alpha-diversity was analyzed by calculating the Chao1 (a proxy for community richness) and Shannon's index (a proxy for diversity, taking into account both richness and evenness). We did not observe differences in bacterial

[1]Departamento de Bioquímica y Biología Molecular, Facultad de Medicina, Instituto Universitario de Oncología (IUOPA), Universidad de Oviedo, Oviedo, Spain. [2]Cell Biology and Metabolomics Platforms, Gustave Roussy Cancer Campus, Villejuif, France. [3]Equipe 11 labellisée par la Ligue contre le Cancer, Centre de Recherche des Cordeliers, Paris, France. [4]INSERM, U1138, Paris, France. [5]Université Paris Descartes, Sorbonne Paris Cité, Paris, France. [6]Unidad de histopatología molecular, IUOPA, Universidad de Oviedo, Oviedo, Spain. [7]Department of Microbiology and Biochemistry of Dairy Products, Instituto de Productos Lácteos de Asturias, Consejo Superior de Investigaciones Científicas (IPLA-CSIC), Villaviciosa, Spain. [8]Diet, Microbiota and Health Group, Instituto de Investigación Sanitaria del Principado de Asturias (ISPA), Oviedo, Spain. [9]Faculty of Health and Sport Sciences, Department of Physiatry and Nursing, University of Zaragoza, Huesca, Spain. [10]GENUD (Growth, Exercise, NUtrition and Development) Research Group, University of Zaragoza, Zaragoza, Spain. [11]Faculty of Sport Science, Universidad Europea de Madrid, Madrid, Spain. [12]Instituto de Investigación Hospital 12 de Octubre (i+12) y Centro de Investigación Biomédica en Red de Fragilidad y Enjevecimiento Saludable (CIBERFES), Madrid, Spain. [13]Université Pierre et Marie Curie, Paris, France. [14]Pôle de Biologie, Hôpital Européen Georges Pompidou, AP-HP, Paris, France. [15]Karolinska Institute, Department of Women's and Children's Health, Karolinska University Hospital, Stockholm, Sweden. [16]Centro de Investigación Biomédica en Red de Cáncer (CIBERONC), Madrid, Spain.
*e-mail: pmquiros@gmail.com; clo@uniovi.es

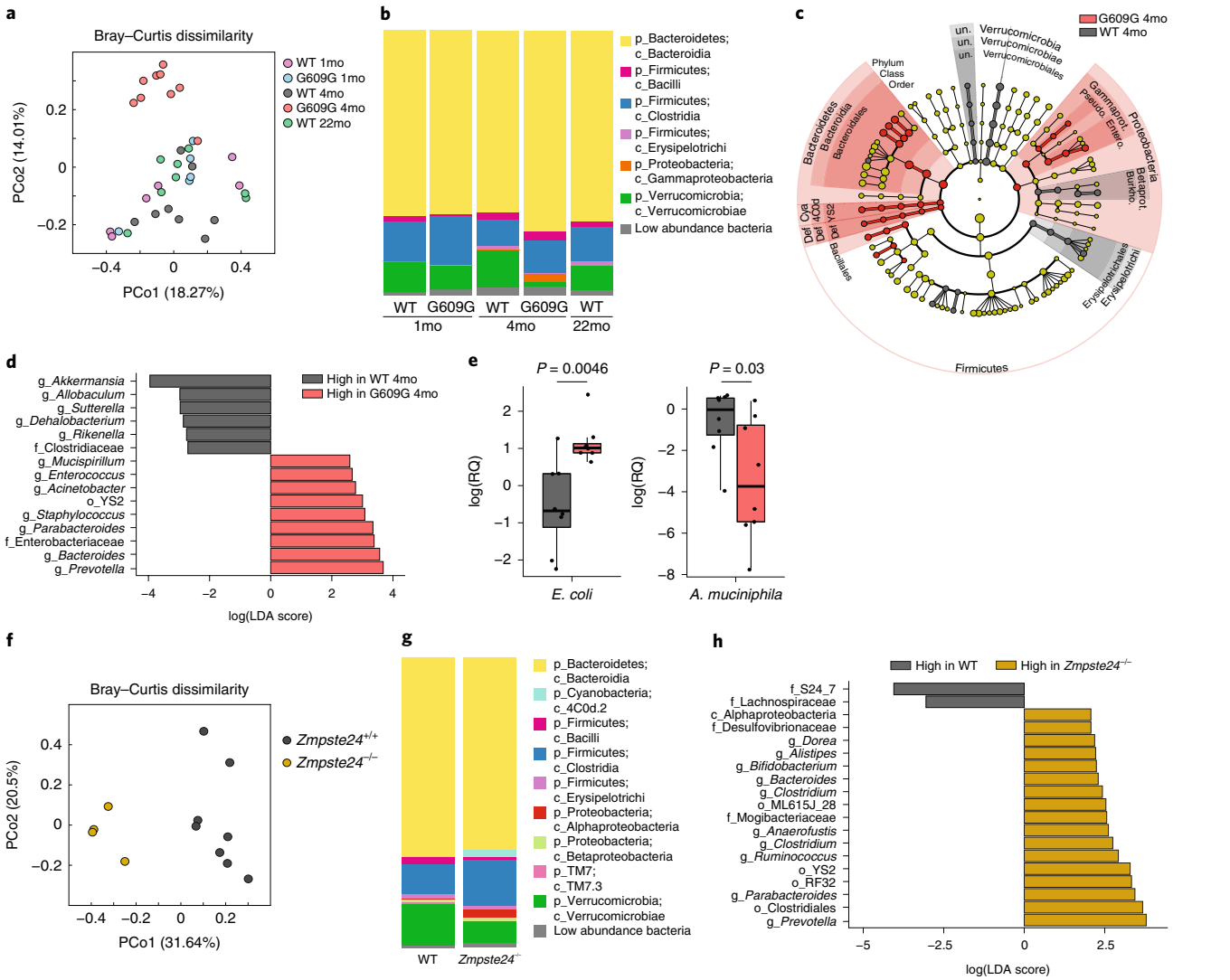

Fig. 1 | Gut dysbiosis in *Lmna*$^{G609G/G609G}$ and *Zmpste24*$^{-/-}$ progeroid mice. a, PCoA of beta-diversity using the Bray–Curtis dissimilarity metric among samples of the five groups of mice analyzed ($P = 0.001$; permutational multivariate analysis of variance, PERMANOVA). G609G 4mo mice show statistical differences with each of the other groups (Supplementary Table 1). Each dot represents an individual mouse. PCo1 and PCo2 represent the percentage of variance explained by each coordinate (WT 1mo, $n = 6$; G609G 1mo, $n = 5$; WT 4mo, $n = 8$; G609G 4mo, $n = 9$; WT 22mo, $n = 8$). **b**, Average relative abundance of prevalent microbiota at the class level in the five groups studied: 1-month-old wild-type (WT 1mo, $n = 6$), 1-month-old *Lmna*$^{G609G/G609G}$ (G609G 1mo, $n = 5$), adult 4-month-old wild-type (WT 4mo, $n = 8$), 4-month-old *Lmna*$^{G609G/G609G}$ (G609G 4mo, $n = 9$) and 22-month-old wild-type (WT 22mo, $n = 8$). The low abundance bacteria group includes all bacterial classes with less than 0.5% of total abundance. **c**, Taxonomic cladogram obtained from LEfSe analysis showing bacterial taxa (phylum, class and order) that were differentially abundant in progeroid and WT mice at 4 months of age. Red indicates increased abundance in progeroid mice; grey indicates increased abundance in WT mice. Def: Deferribacteres (phylum), Deferribacteres (order), Deferribacterales (class); Cya: Cyanobacteria (phylum); Pseudo: Pseudomonadales; Entero: Enterobacteriales; Burkho: Burkholderiales. **d**, Results of LEfSe analysis showing bacterial taxa that were significantly different in abundance between G609G and WT mice at 4 months of age. For **c** and **d**, WT 4mo, $n = 8$; G609G 4mo, $n = 9$. **e**, Validation using quantitative polymerase chain reaction (qPCR) of the differences in abundance of *Escherichia coli* (Wilcoxon test statistic (W) = 6, $P = 0.0046$) and *A. muciniphila* ($W = 52$, $P = 0.03$) between WT ($n = 8$) and G609G mice ($n = 8$) at 10 weeks of age. Two-tailed unpaired Wilcoxon rank-sum test. Each dot represents an individual mouse. In the box plots, upper and lower hinges correspond to the first and third quartiles, the center line represents the median, whiskers indicate the highest and lowest values that are within 1.5 × IQR, and data beyond the end of the whiskers are outliers and plotted as points. RQ, relative quantification. **f**, PCoA of beta-diversity using the Bray–Curtis dissimilarity metric between *Zmpste24*$^{-/-}$ and WT mice ($P = 0.003$, PERMANOVA). Each dot represents an individual mouse. PCo1 and PCo2 represent the percentage of variance explained by each coordinate. **g**, Average relative abundance of prevalent microbiota at the class level in WT and *Zmpste24*$^{-/-}$ mice. **h**, LEfSe analysis showing bacterial taxa that were significantly different in abundance between *Zmpste24*$^{-/-}$ and WT mice. LDA, linear discriminant analysis. For **f**–**h**, 4-month-old WT mice, $n = 8$ (same as **a**–**d**); 4-month-old *Zmpste24*$^{-/-}$ mice, $n = 4$. p, phylum; c, class; o, order; f, family; g, genus.

diversity or richness within any of the mouse groups (Extended Data Fig. 1b,c and Supplementary Table 1). Next, we evaluated the beta-diversity across mouse groups, identifying a differential clustering of *Lmna*$^{G609G/G609G}$ 4mo mice in a principal coordinates analysis (PCoA) using the Bray–Curtis dissimilarity (qualitative measure) (Fig. 1a) and Jaccard distances (quantitative measure) (Extended Data Fig. 1d).

Similar differences were revealed by hierarchical clustering, where *Lmna*$^{G609G/G609G}$ 4mo mice were grouped together and separated from all other groups (Extended Data Fig. 1e,f).

Next, we calculated the percentage of bacterial taxa in each group (Fig. 1b and Extended Data Fig. 2a), applying a linear discriminant analysis effect size (LEfSe) method (see Methods; Supplementary Table 2). We noted a similar profile for WT and *Lmna*$^{G609G/G609G}$ mice at 1 month of age (Fig. 1b and Extended Data Fig. 2a), observing only an increment in the genera *Allobaculum* from the family Erysipelotrichaceae, *Desulfovibrio* (class Deltaproteobacteria) and Clostridiales of the families Ruminococcaceae and Lachnospiraceae, in *Lmna*$^{G609G/G609G}$ 1mo mice (Extended Data Fig. 2b). As WT mice aged (from 1 to 4 months), we noted an increment in genera such as *Allobaculum*, *Ruminococcus*, *Coprococcus*, *Turicibacter* or *Parabacteroides* (Extended Data Fig. 2c); however, the changes from 1 to 4 months were more profound in progeroid mice, which displayed a loss in *Akkermansia* and *Dehalobacterium* and an enrichment in *Parabacteroides*, *Prevotella* and the Enterobacteriaceae, among other differences (Extended Data Fig. 2d). When comparing WT and progeroid mice at 4 months of age, the pattern was substantially different (Fig. 1b,c and Extended Data Fig. 2a), in agreement with the progression of the aging phenotype. The main differences were a reduction in abundance of Erysipelotrichales (phylum Firmicutes), Burkholderiales (class Betaproteobacteria) and Verrucomicrobiales (phylum Verrucomicrobia) in progeroid mice, together with an increase in Bacteroidales (phylum Bacteroidetes), Deferribacterales (phylum Deferribacteres), YS2 (phylum Cyanobacteria) and the Proteobacteria Enterobacteriales and Pseudomonadales (class Gammaproteobacteria) (Fig. 1c and Supplementary Table 2). At a lower taxonomical level, *Lmna*$^{G609G/G609G}$ 4mo mice showed a loss in Clostridiaceae, *Allobaculum*, *Sutterella*, *Dehalobacterium*, *Rikenella* and *Akkermansia* (Fig. 1d). Of note, a high abundance of *Akkermansia* has been associated with improved immunomodulation and metabolic homeostasis, reduced inflammation and protection against atherosclerosis[17–19]. By contrast, *Lmna*$^{G609G/G609G}$ 4mo exhibited an increment in *Mucispirillum*, *Enterococcus*, *Acinetobacter*, *Staphylococcus*, *Parabacteroides*, *Bacteroides*, *Prevotella* and Enterobacteriaceae, which contains the genus *Escherichia* and has been associated with dysbiosis and intestinal inflammation[20] (Fig. 1d). Changes in *Escherichia* and *Akkermansia* were validated afterwards at the species level by qPCR in a second, independent group of *Lmna*$^{G609G/G609G}$ mice (Fig. 1e). The gut microbiome of a fraction of WT 22mo mice exhibited a tendency towards intestinal dysbiosis (Extended Data Fig. 2a); however, the only significant shift consisted in the loss in *Rikenella* (Extended Data Fig. 2e), a change also found when comparing *Lmna*$^{G609G/G609G}$ 4mo to WT 4mo mice (Fig. 1d). To explore the functional implications of the microbiome shift in progeroid mice, we then investigated the metagenome data with PICRUSt and HUMAnN2 (see Methods). LEfSe analysis detected an increase in KEGG pathways related to pathological bacteria such as 'Bacterial invasion of epithelial cells' (ko05100) and 'Flagellar assembly' (ko02040), and a differential enrichment in multiple metabolic pathways (Extended Data Fig. 2f and Supplementary Table 3).

To confirm the association of gut dysbiosis with progeria, we analyzed the gut microbiota of a different progeria model, *Zmpste24*$^{-/-}$ mice[21] (Extended Data Fig. 3a). Although *Zmpste24*$^{-/-}$ mice showed no differences in bacterial diversity (Extended Data Fig. 3b), they exhibited higher bacterial richness (Extended Data Fig. 3c). Like *Lmna*$^{G609G/G609G}$ mice, *Zmpste24*$^{-/-}$ animals showed differences in beta-diversity at quantitative (Fig. 1f) and qualitative (Extended Data Fig. 3d) levels, clustering differently from WT mice, and exhibited signs of dysbiosis (Fig. 1g and Extended Data Fig. 3e) with a high abundance of Proteobacteria (class Alphaproteobacteria) and Cyanobacteria (Fig. 1g, Extended Data Fig. 3e and Supplementary Table 2). *Zmpste24*$^{-/-}$ mice also showed a tendency to a lower amount of Verrucomicrobia (Extended Data Fig. 3e), although this trend was less marked than in *Lmna*$^{G609G/G609G}$ animals, perhaps due to the later onset of the progeroid phenotype in *Zmpste24*$^{-/-}$ mice. At a lower taxonomic level, we found, among other differences, an enrichment in the order YS2 (phylum Cyanobacteria) and the genera *Bacteroides*, *Parabacteroides* and *Prevotella* (Fig. 1h), similarly to *Lmna*$^{G609G/G609G}$ 4mo mice.

To investigate the possible existence of gut dysbiosis in human progeria, we obtained fecal samples from four children with HGPS and their healthy siblings, as well as from a patient with NGPS and his healthy sibling and mother (Extended Data Fig. 4a). When comparing progeria patients with their healthy controls, we found no differences in the alpha-diversity (Extended Data Fig. 4b,c) or beta-diversity indices (Fig. 2a and Extended Data Fig. 4d). However, when samples were compared by geographical location (that is, comparing families), a differential clustering was observed at the quantitative (Fig. 2b) and qualitative (Extended Data Fig. 4e) levels. Despite the low number of samples, these results suggest that the environment has more influence on the gut microbiome than the pathological condition, which is in accordance with recent findings[22,23]. Yet, in each of the studied families, the progeria patients had a different profile compared to their healthy siblings. This was particularly evident in families where more than one healthy member was studied (Extended Data Fig. 4f). LEfSe analysis pointed to a loss in *Gemmiger*—family Ruminococcaceae—and an enrichment in *Clostridium* from the families Erysipelotrichaceae and Lachnospiraceae in progeria patients (Fig. 2c).

Considering the gut microbiome alterations observed in mice and progeria patients, we hypothesized that individuals with exceptionally long lifespans (that is, centenarians) might possess a health-promoting microbiome. We thus performed a metagenomic analysis of a centenarian cohort and ethnically matched healthy adult controls (Extended Data Fig. 5a). Centenarians showed lower alpha-diversity compared to their controls (Extended Data Fig. 5b), and a considerably lower bacterial richness (Extended Data Fig. 5c). Also, both groups clustered differentially, based on quantitative (Fig. 2d) and qualitative (Extended Data Fig. 5d) beta-diversity indices, indicating that centenarians had a different microbial community structure than controls. Indeed, we encountered distinct microbial profiles in both groups (Fig. 2e and Extended Data Fig. 5e). LEfSe analysis showed that centenarians presented less Betaproteobacteria and more Synergistia and Verrucomicrobiae, among others (Fig. 2e and

Fig. 2 | Alterations in the gut microbiome in progeria patients and long-lived humans. a,**b**, PCoA of beta-diversity using the Bray–Curtis dissimilarity metric among fecal samples analyzed by health status ($P=0.5$, PERMANOVA) (Control, $n=9$ individuals; Progeria, $n=5$ individuals) (**a**) and family ($P=0.001$, PERMANOVA) (Family A, $n=3$; Family B, $n=3$; Family C, $n=3$; Family D, $n=2$; Family E, $n=3$) (**b**). Each dot represents one person. PCo1 and PCo2 represent the percentage of variance explained by each coordinate. **c**, Results of LEfSe analysis showing bacterial genera whose abundance significantly differed between progeria patients and their healthy siblings (Control = 9 individuals; Progeria = 5 individuals). **d**, PCoA of beta-diversity using the Bray–Curtis dissimilarity metric of healthy controls (HC; $n=14$ individuals) and centenarians (Ce; $n=17$ individuals) ($P=0.001$, PERMANOVA). Each dot represents one person. **e**, Average relative abundance of prevalent microbiota at the class level in centenarians (Ce; $n=17$ individuals) and healthy controls (HC; $n=14$ individuals). The low abundance bacteria group includes all bacterial classes with less than 0.5% of total abundance. **f**, Results of LEfSe analysis showing bacteria, at the lowest taxonomic level, that were significantly different in abundance in centenarians (Ce; $n=17$ individuals) versus healthy controls (HC; $n=14$ individuals). p, phylum; c, class; o, order; f, family; g, genus.

Supplementary Table 2). At a lower taxonomic level, centenarians were characterized by a lower abundance of Desulfovibrionaceae, Lachnospiraceae and Erysipelotrichaceae—the last two enriched in progeria patients—and *Prevotella*, *Sutterella*, *Roseburia or Butyricicoccus*, among other differences (Fig. 2f). Notably, centenarians exhibited a higher abundance of Enterobacteriaceae, Ruminococcaceae and Christensenellaceae and the genera *Klebsiella*, *Lactobacillus*, *Parabacteroides* and *Akkermansia* (Fig. 2f).

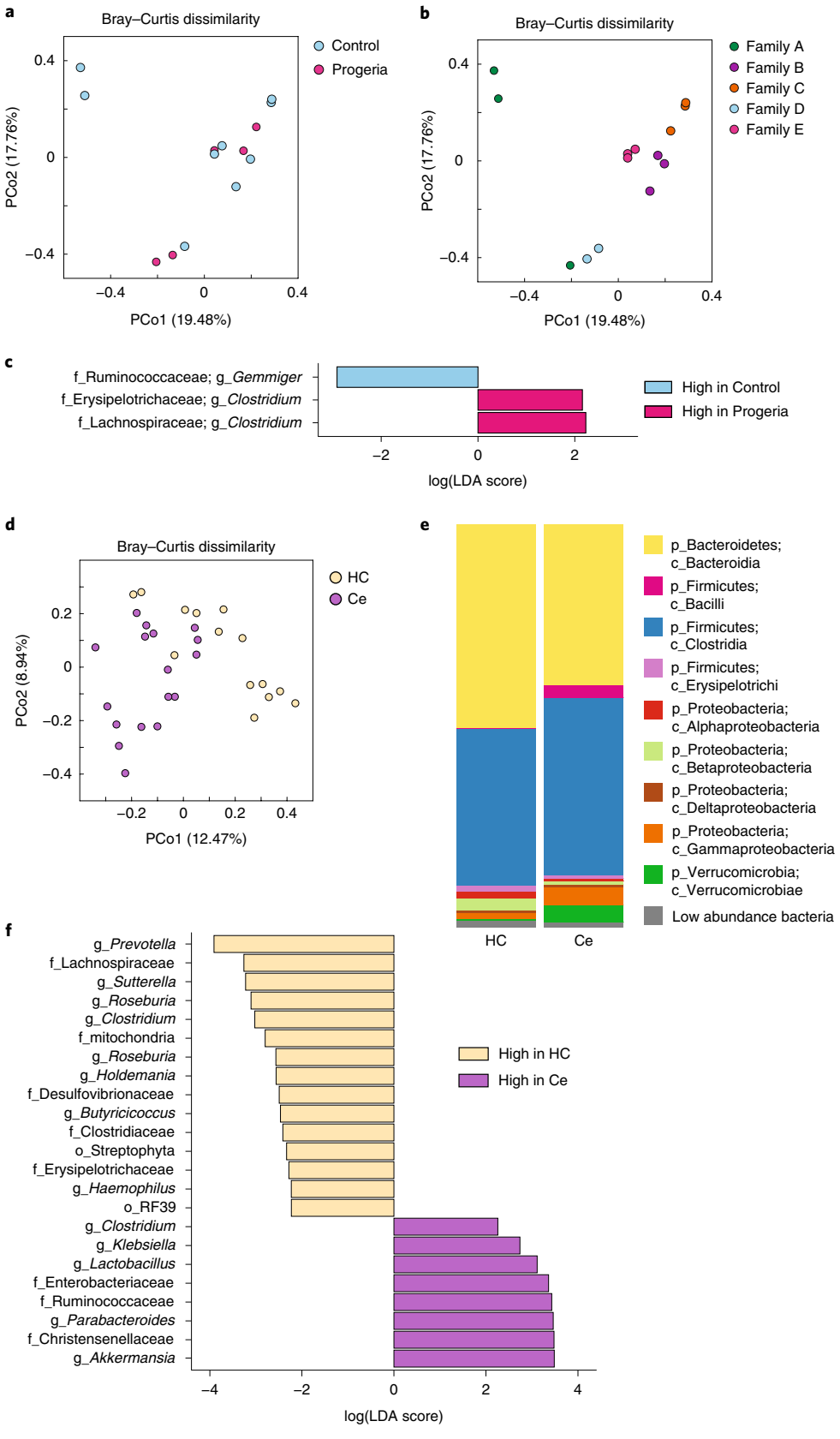

These results are in line with previous studies reporting high levels of *Akkermansia* and Christensenellaceae and low levels of *Roseburia* in centenarians[12,24].

Based on the aforementioned results, we hypothesized that changes in the gut microbiota might accompany the accelerated aging of HGPS mice. To explore this possibility, we performed FMT in four different mouse groups. First, we used WT control mice as microbiota donors (herein referred to as WTmic, *WT microbiota*) and *Lmna*$^{G609G/G609G}$ mice as recipients. We also transplanted *Lmna*$^{G609G/G609G}$ mice with microbiota from older *Lmna*$^{G609G/G609G}$ mice, that is, progeroid mice with a more advanced phenotype (oG609Gmic, *old Lmna*$^{G609G/G609G}$ microbiota) (Fig. 3a). FMT effectiveness was evaluated by comparing the gut metagenomic profiles of control, transplanted and donor mice, showing that transplanted progeroid mice acquired the donor microbiota (Extended Data Fig. 6a,b). Additionally, we performed microbiome ablation and sham-transplanted *Lmna*$^{G609G/G609G}$ mice (herein referred to as EmptyT, *empty transplant*) (Fig. 3a). *Lmna*$^{G609G/G609G}$-WTmic manifested a delayed loss of body weight and temperature (Fig. 3b,c). Phenotype-dependent hypoglycemia was avoided and renal perivascular fibrosis was attenuated in *Lmna*$^{G609G/G609G}$-WTmic (Fig. 3d,e). Spleen weight, typically reduced in progeroid mice, was similar in *Lmna*$^{G609G/G609G}$-WTmic and *Lmna*$^{G609G/G609G}$ controls, but lower in *Lmna*$^{G609G/G609G}$-oG609Gmic (Extended Data Fig. 6c). We also noted an increase in intestinal inflammation markers in *Lmna*$^{G609G/G609G}$ mice that was recovered in *Lmna*$^{G609G/G609G}$-WTmic (Extended Data Fig. 6d). Surprisingly, some markers were also decreased in *Lmna*$^{G609G/G609G}$-oG609Gmic, pointing to a possible beneficial effect of the FMT protocol per se (Extended Data Fig. 6d). Most importantly, *Lmna*$^{G609G/G609G}$-WTmic showed improved survival compared to control *Lmna*$^{G609G/G609G}$ mice ($P=0.0029$), with a 13.5% increase in median lifespan (160 versus 141 days, respectively) (Fig. 3f). *Lmna*$^{G609G/G609G}$-WTmic also exhibited an extended maximal survival (9% increment, $P=0.04$) (Fig. 3f and Extended Data Fig. 6e). In contrast, *Lmna*$^{G609G/G609G}$-oG609Gmic showed reduced survival compared to control *Lmna*$^{G609G/G609G}$ mice ($P=0.045$), with a reduction in median lifespan (129 days) (Fig. 3f). *Lmna*$^{G609G/G609}$ -EmptyT did not show survival differences when compared to control *Lmna*$^{G609G/G609G}$ mice (Extended Data Fig. 6f). Finally, to evaluate the potential pathogenicity of progeroid microbiota, we also performed FMT from aged *Lmna*$^{G609G/G609G}$ donors into WT mice (WT-oG609Gmic). Effective gut colonization was validated by comparing the metagenomic profiles of control, transplanted and donor mice (Extended Data Fig. 6a,b). We did not observe progeria-related features in WT-oG609Gmic mice. However, this maneuver caused metabolic alterations, including a higher body weight, higher glucose levels, lower O_2 consumption, lower CO_2 production and reduced energy expenditure (Fig. 3g–k and Extended Data Fig. 7a–d).

To validate these results, we also performed FMT in *Zmpste24*$^{-/-}$ mice using microbiota from WT mice (*Zmpste24*$^{-/-}$-WTmic). This manipulation caused *Zmpste24*$^{-/-}$ mice to manifest a less pronounced cervicothoracic lordokyphosis, larger body size and maintained grooming (Fig. 3l). Body weight loss (Fig. 3m and Extended Data Fig. 8a) and hypoglycemia (Fig. 3n)

Fig. 3 | Effects of fecal microbiota transplantation in progeroid and WT mice. a, Scheme of the experimental design, in which the effects of FMT were assessed using four different groups of progeroid mice: control untransplanted *Lmna*$^{G609G/G609G}$ mice ($n=11$), *Lmna*$^{G609G/G609G}$ mice transplanted with fecal microbiota from WT mice (*Lmna*$^{G609G/G609G}$-WTmic; $n=11$), *Lmna*$^{G609G/G609G}$ mice transplanted with microbiota from older *Lmna*$^{G609G/G609G}$ mice (*Lmna*^{G609G}-oG609Gmic; $n=11$) and *Lmna*$^{G609G/G609G}$ mice subjected to ablation of their own microbiota and transplanted with empty buffer (*Lmna*^{G609G}-EmptyT; $n=8$). Transplants were carried on at ~8 to 10 weeks of age, using as donors 4-month-old WT and 4-month-old *Lmna*$^{G609G/G609G}$ mice. **b**, Comparison of the percentage of initial body weight between *Lmna*$^{G609G/G609G}$ ($n=11$) and *Lmna*$^{G609G/G609G}$-WTmic ($n=11$) mice over the indicated time period. Differences in body weight over time were assessed with a linear mixed model and analyzed with an analysis of variance (ANOVA) type II Wald chi-squared test ($\chi^2=8.06$, d.f. = 1, $P=0.0045$). Data are presented as mean ± s.e.m. **c**, Box plots showing differences in body temperature between WT ($n=4$), *Lmna*$^{G609G/G609G}$ ($n=6$) and *Lmna*$^{G609G/G609G}$-WTmic ($n=5$) mice. One-way ANOVA with Tukey's correction ($F=20.45$, d.f. = 2, $P=0.0001$). Exact adjusted *P* values are reported within the plot. **d**, Comparison of the glucose levels between *Lmna*$^{G609G/G609G}$ ($n=6$) and *Lmna*$^{G609G/G609G}$-WTmic ($n=5$) mice over the indicated time period. Unpaired two-tailed Student's *t*-test (for week 5: $t=2.74$, d.f. = 36, $P=0.009$). **e**, Representative histological images of renal vasculature, showing increased perivascular fibrosis in *Lmna*$^{G609G/G609G}$ mice ($n=10$) (blue staining, indicated with an arrow) compared to WT ($n=10$) and *Lmna*$^{G609G/G609G}$ mice transplanted with WT microbiota (*Lmna*^{G609G}-WTmic; $n=8$). Renal fibrosis scores were analyzed with a Kruskal–Wallis test with Dunn's correction. Exact adjusted *P* values are reported within the plot. Each dot represents a single mouse. The horizontal line represents the mean ± 95% confidence interval (CI). Scale bar, 100 µm. **f**, Per cent survival of *Lmna*$^{G609G/G609G}$ ($n=11$), *Lmna*$^{G609G/G609G}$-WTmic ($n=11$) and *Lmna*$^{G609G/G609G}$ mice transplanted with old *Lmna*$^{G609G/G609G}$ microbiota (*Lmna*^{G609G}-oG609Gmic; $n=11$). Differences were analyzed with the log-rank Mantel–Cox test and Benjamini–Hochberg (BH) correction was applied after pairwise comparisons between all experimental groups, including Empty transplant (Extended Data Fig. 6f). The hazard ratio (HR) was calculated using a Cox proportional model. For *Lmna*$^{G609G/G609G}$-WTmic versus *Lmna*$^{G609G/G609G}$, HR of 0.2 (95% CI 0.07–0.53), $P=0.0012$; for *Lmna*$^{G609G/G609G}$-oG609Gmic versus *Lmna*$^{G609G/G609G}$, HR of 4.1 (95% CI 1.5–11.1), $P=0.005$. Median and maximal survival, percentage of median and maximal lifespan extension and log-rank test adjusted *P* values are indicated in the Kaplan–Meier plot. Transplantation was performed starting at ~8 to 10 weeks of age. **g**, Comparison of body weight between male WT mice transplanted with progeroid microbiota (WT-oG609Gmic; $n=7$) and male WT controls ($n=7$) over the indicated time period. Differences of body weight over time were assessed with a linear mixed model and analyzed with an ANOVA type II Wald χ^2 test ($\chi^2=5.49$, d.f. = 1, $P=0.019$). Data are presented as mean ± s.e.m. **h**, Blood glucose levels of WT-Ctrl mice ($n=14$; 7 males and 7 females) and WT-oG609Gmic ($n=14$; 7 males and 7 females). Unpaired two-tailed Student's *t*-test ($t=4.56$, d.f. = 26, $P=0.0001$). Each dot represents a single mouse. The horizontal line represents the mean ± 95% CI. **i**–**k**, Metabolic parameters, measured with an Oxymax system, of WT-Ctrl ($n=14$; 7 males and 7 females) and WT-oG609Gmic ($n=14$; 7 males and 7 females) mice (differences were analyzed with an unpaired two-tailed Welch's *t*-test): volume of O_2 consumed (**i**, V_{O2}) ($t=2.71$, d.f. = 28, $P=0.011$); volume of CO_2 produced (**j**, V_{CO2}) ($t=3.94$, d.f. = 23, $P=0.0006$); energy expenditure (**k**, EE) ($t=3.15$, d.f. = 25, $P=0.0043$). **l**, Representative pictures of control *Zmpste24*$^{-/-}$ mice and *Zmpste24*$^{-/-}$ mice transplanted with WT microbiota (*Zmpste24*$^{-/-}$-WTmic). Transplanted mice appear to be healthier, as manifested by an ameliorated cervicothoracic lordokyphosis, a larger size and better grooming. **m**, Body weight at 35 weeks of life of *Zmpste24*$^{-/-}$ mice ($n=4$) and *Zmpste24*$^{-/-}$-WTmic mice ($n=6$). Unpaired two-tailed Student's *t*-test ($t=4.31$, d.f. = 8, $P=0.0026$). **n**, Blood glucose levels of *Zmpste24*$^{-/-}$ mice ($n=5$) and *Zmpste24*$^{-/-}$-WTmic mice ($n=7$) at 30 weeks. Unpaired two-tailed Student's *t*-test ($t=5.47$, d.f. = 11, $P=0.0002$). **o**, Per cent survival of *Zmpste24*$^{-/-}$ ($n=7$) and *Zmpste24*$^{-/-}$-WTmic female mice ($n=7$). Differences were performed with the log-rank Mantel–Cox test ($P=0.0092$). HR of 0.15 (95% CI 0.03–0.75), $P=0.021$. Median and maximal survival, percentage of median and maximal lifespan extension and exact *P* value are indicated in the Kaplan–Meier plot. Transplantation was performed starting at ~7 to 10 weeks of age. For **c**, **d**, **i**–**k**, **m** and **n**, box plots show upper and lower hinges corresponding to the first and third quartiles, center line represents the median, whiskers indicate the highest and lowest values that are within 1.5 × IQR, and data beyond the end of the whiskers are outliers and plotted as points. Each dot represents a single mouse.

were avoided in *Zmpste24*$^{-/-}$-WTmic mice. Like *Lmna*$^{G609G/G609G}$ mice transplanted with WT microbiota, *Zmpste24*$^{-/-}$-WTmic mice also exhibited enhanced survival ($P=0.0092$), with a median lifespan increase of 13.4% (279 versus 246 days) (Fig. 3o). Maximum survival was increased by almost 8% ($P=0.09$) (Fig. 3o and Extended Data Fig. 8b).

The results above in both human and murine gut metagenomic profiles described a loss in *A. muciniphila* in *Lmna*$^{G609G/G609G}$ 4mo mice and an increase in centenarians' samples. Because this bacterium exerts beneficial effects in other models[17,19,25,26], we tested if an external supply of *A. muciniphila* to *Lmna*$^{G609G/G609G}$ mice would improve their healthspan or lifespan. By supplementing *Lmna*$^{G609G/G609G}$ mice with *A. muciniphila* through oral gavage, we obtained a modest lifespan extension ($P=0.016$) (Fig. 4a), suggesting a protective role of this microorganism against accelerated aging manifestations. As previously described[19], *A. muciniphila* supplementation induced ileal expression of *Reg3g* (Fig. 4b) and favored the thickening of the intestinal mucosa layer (Fig. 4c). *Lmna*$^{G609G/G609G}$ mice receiving *A. muciniphila* also showed an increment in the intestinal trefoil factor *Tff3* (Fig. 4b), which might promote wound healing and repair of the mucosa layer[27].

Finally, to investigate the potential mechanisms accounting for the healthspan and lifespan extension of *Lmna*$^{G609G/G609G}$ mice after FMT, we performed metabolome profiling of the ileal content from WT, *Lmna*$^{G609G/G609G}$ and *Lmna*$^{G609G/G609G}$-WTmic mice. Significant changes were analyzed by metabolite set enrichment analysis using KEGG pathways, detecting an enrichment in 'secondary bile acid biosynthesis' (Fig. 4d). As recently described[28], different bile acids were decreased in *Lmna*$^{G609G/G609G}$ compared to WT mice, and recovered in *Lmna*$^{G609G/G609G}$-WTmic (Fig. 4e). Moreover, *Lmna*$^{G609G/G609G}$ mice ileal content exhibited a depletion of the monosaccharides arabinose and ribose, the nucleoside inosine and the ether-phospholipid PCae (18:0), which was reversed upon FMT with WT microbiota (Fig. 4f).

FMT might modulate obesity and metabolism in humans and mice[29,30], ameliorate metabolic syndrome in patients[31] and contribute

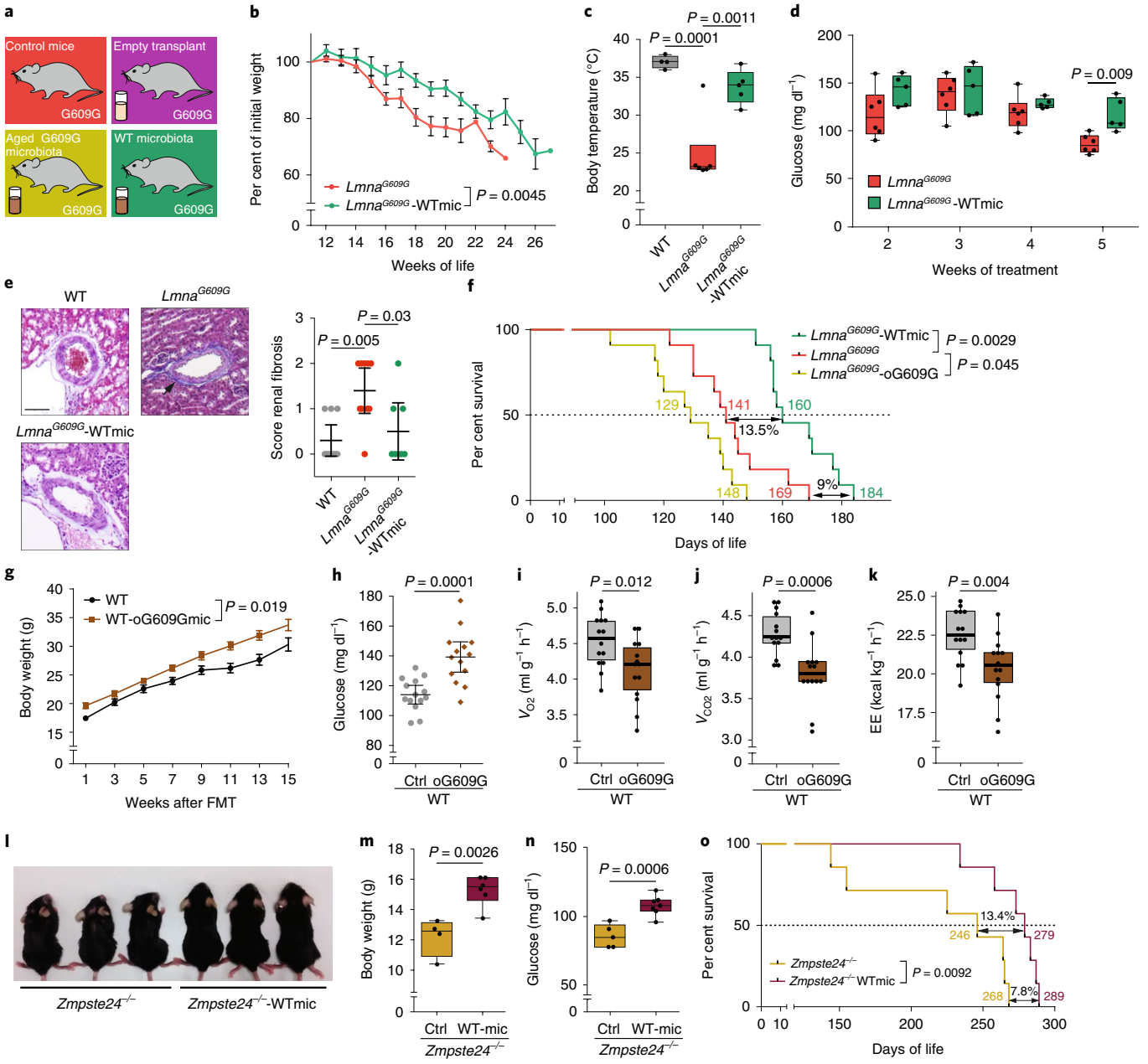

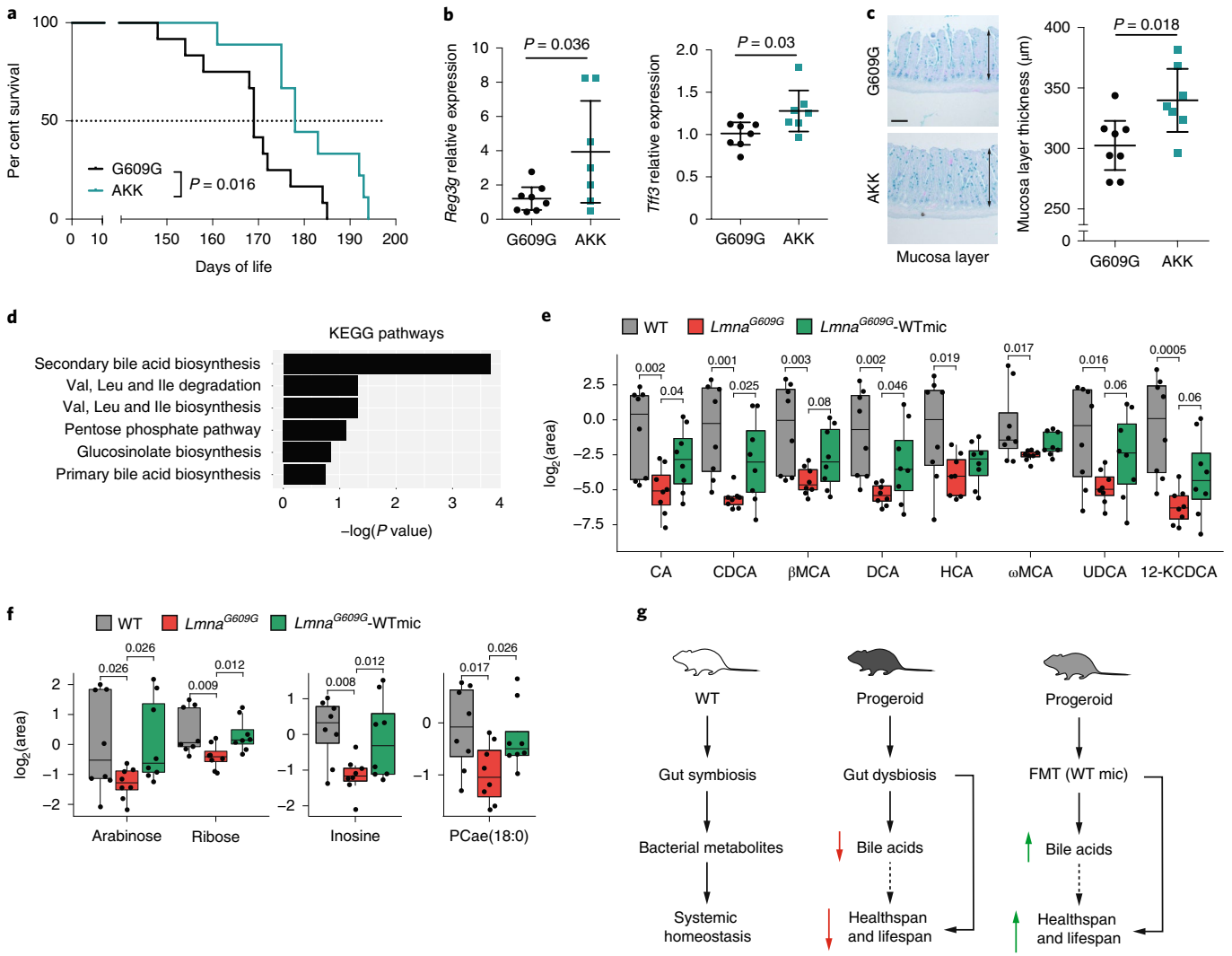

Fig. 4 | *A. muciniphila* supplementation in progeroid mice and metabolomic analysis of ileal content. a, Per cent survival of $Lmna^{G609G/G609G}$ mice receiving *A. muciniphila* by oral gavage (AKK; $n=9$) compared to $Lmna^{G609G/G609G}$ mice (G609G; $n=12$). *A. muciniphila* transplantation was performed starting at 7 to 8 weeks of age. Differences in survival were analyzed with the log-rank Mantel–Cox test ($P=0.0163$). HR was calculated using a Cox proportional model (HR of 0.31 (95% CI 0.11–0.86), $P=0.0244$). **b**, Relative expression levels of *Reg3g* and *Tff3* in G609G ($n=8$) and AKK ($n=7$) mice. Differences were analyzed with an unpaired two-tailed Student's *t*-test. For *Reg3g*, $t=2.33$, d.f. $=13$, $P=0.0365$; for *Tff3*, $t=2.42$, d.f. $=13$, $P=0.0306$. Data are represented as dots (one per mouse) with mean ± 95% CI. **c**, Left, representative histological images of the intestinal mucosa layer of G609G and AKK mice. Arrows indicate the thickness of the mucosa layer. Scale bar, 100 μm. Right, comparison of mucosa layer thickness of G609G ($n=8$) and AKK ($n=7$) mice. Differences were calculated using an unpaired two-tailed Welch's *t*-test ($t=2.72$, d.f. $=12$, $P=0.018$). Data are represented as dots (one per mouse) with mean ± 95% CI. For **b** and **c**, the G609G group comprised four males and four females, and the AKK group comprised four males and three females. **d**, Metabolic set enrichment analysis of all metabolites with statistically significant differences between the three groups: WT ($n=8$), $Lmna^{G609G/G609}$ ($n=8$) and $Lmna^{G609G/G609G}$-WTmic ($n=8$), using all annotated KEGG pathways (see Methods). **e**, Box plots showing the relative levels of different bile acids in WT ($n=8$), $Lmna^{G609G/G609}$ ($n=8$) and $Lmna^{G609G/G609G}$-WTmic ($n=8$). CA, cholic acid; CDCA, chenodeoxycholic acid; βMCA, beta-muricholic acid; DCA, deoxycholic acid; HCA, hyocholic acid; ωMCA, omega-muricholic acid; UDCA, ursodeoxycholic acid; 12-KCDCA, 12-ketochenodeoxycholic acid. **f**, Box plots showing the relative levels of selected metabolites between WT ($n=8$), $Lmna^{G609G/G609G}$ ($n=8$) and $Lmna^{G609G/G609G}$-WTmic ($n=8$). For **e** and **f**, each group of eight mice comprised four males and four females. In both panels, differences were analyzed using a one-way ANOVA with multiple comparison test with one-side relative to control $Lmna^{G609G/G609G}$ mice. Exact adjusted *P* values are reported in each plot. In the box plots, upper and lower hinges correspond to the first and third quartiles, the center line represents the median, whiskers indicate the highest and lowest values that are within 1.5 × IQR, and data beyond the end of the whiskers are outliers and plotted as points. Each dot represents a single mouse. **g**, Schematic representation of the model proposed in this work. WT mice are characterized by a gut symbiosis in which bacterial metabolites participate in systemic homeostasis. By contrast, progeroid mice are characterized by a gut dysbiosis, leading to decreased bile acid levels and a reduced healthspan and lifespan. FMT of WT microbiota (WT mic) into progeroid mice raises bile acids levels and improves healthspan and lifespan.

to the treatment of refractory immune checkpoint inhibitor-associated colitis[32] and recurrent infections by *Clostridium difficile*[33]. The promising in vivo results obtained in this study suggest that therapeutic interventions on the intestinal microbiome may lead to healthspan end even lifespan improvements. In this regard, we show that *A. muciniphila* administration leads to a lifespan enhancement in progeria, thus extending previous findings on the pro-health activities of *Akkermansia* spp. in the intestinal tract of mammals[17–19] and in

aged mice[34]. Previous studies have described that successful FMT treatment of recurrent infection by *C. difficile* relies on restoration of correct bile acid metabolism[35,36], and that antibiotic-induced microbiome depletion reduces the secondary bile acid pool[37]. Of note, secondary bile acids are produced by the gut microbiota[38] and positively correlate with *Akkermansia* levels in mice[39]. Considering that bile acids regulate metabolism and anti-inflammatory signals[40] and that they are depleted in *Lmna*$^{G609G/G609G}$ mice[28], the restoration of secondary bile acids—and other metabolites (arabinose, ribose, inosine)—by FMT might contribute to extend healthspan and lifespan in progeroid mice (Fig. 4g). Future work might identify the functional mechanisms by which some bacterial species and metabolites are responsible for the healthspan and lifespan extension conferred by FMT, and explore the applicability of FMT in normal or accelerated aging.

Online content

Any methods, additional references, Nature Research reporting summaries, source data, statements of code and data availability and associated accession codes are available at https://doi.org/10.1038/s41591-019-0504-5.

Received: 16 November 2017; Accepted: 30 May 2019;
Published online: 22 July 2019

References

1. Thaiss, C. A., Zmora, N., Levy, M. & Elinav, E. The microbiome and innate immunity. *Nature* **535**, 65–74 (2016).
2. Leulier, F. et al. Integrative physiology: at the crossroads of nutrition, microbiota, animal physiology and human health. *Cell Metab.* **25**, 522–534 (2017).
3. Koeth, R. A. et al. Intestinal microbiota metabolism of L-carnitine, a nutrient in red meat, promotes atherosclerosis. *Nat. Med.* **19**, 576–585 (2013).
4. Loomba, R. et al. Gut microbiome-based metagenomic signature for non-invasive detection of advanced fibrosis in human nonalcoholic fatty liver disease. *Cell Metab.* **25**, 1054–1062 (2017).
5. Qin, J. et al. A metagenome-wide association study of gut microbiota in type 2 diabetes. *Nature* **490**, 55–60 (2012).
6. Zitvogel, L., Daillere, R., Roberti, M. P., Routy, B. & Kroemer, G. Anticancer effects of the microbiome and its products. *Nat. Rev. Microbiol.* **15**, 465–478 (2017).
7. Cabreiro, F. & Gems, D. Worms need microbes too: microbiota, health and aging in *Caenorhabditis elegans*. *EMBO Mol. Med.* **5**, 1300–1310 (2013).
8. Rios-Covian, D. et al. Intestinal short chain fatty acids and their link with diet and human health. *Front. Microbiol.* **7**, 185 (2016).
9. Breton, J. et al. Gut commensal *E. coli* proteins activate host satiety pathways following nutrient-induced bacterial growth. *Cell Metab.* **23**, 324–334 (2016).
10. Wahlstrom, A., Sayin, S. I., Marschall, H. U. & Backhed, F. Intestinal crosstalk between bile acids and microbiota and its impact on host metabolism. *Cell Metab.* **24**, 41–50 (2016).
11. Schroeder, B. O. & Backhed, F. Signals from the gut microbiota to distant organs in physiology and disease. *Nat. Med.* **22**, 1079–1089 (2016).
12. Biagi, E. et al. Gut microbiota and extreme longevity. *Curr. Biol.* **26**, 1480–1485 (2016).
13. O'Toole, P. W. & Jeffery, I. B. Gut microbiota and aging. *Science* **350**, 1214–1215 (2015).
14. Gordon, L. B., Rothman, F. G., Lopez-Otin, C. & Misteli, T. Progeria: a paradigm for translational medicine. *Cell* **156**, 400–407 (2014).
15. Puente, X. S. et al. Exome sequencing and functional analysis identifies BANF1 mutation as the cause of a hereditary progeroid syndrome. *Am. J. Hum. Genet.* **88**, 650–656 (2011).
16. Osorio, F. G. et al. Splicing-directed therapy in a new mouse model of human accelerated aging. *Sci. Transl. Med.* **3**, 106ra107 (2011).
17. Plovier, H. et al. A purified membrane protein from *Akkermansia muciniphila* or the pasteurized bacterium improves metabolism in obese and diabetic mice. *Nat. Med.* **23**, 107–113 (2017).
18. Schneeberger, M. et al. *Akkermansia muciniphila* inversely correlates with the onset of inflammation, altered adipose tissue metabolism and metabolic disorders during obesity in mice. *Sci. Rep.* **5**, 16643 (2015).
19. Everard, A. et al. Cross-talk between *Akkermansia muciniphila* and intestinal epithelium controls diet-induced obesity. *Proc. Natl Acad. Sci. USA* **110**, 9066–9071 (2013).
20. Maharshak, N. et al. Altered enteric microbiota ecology in interleukin 10-deficient mice during development and progression of intestinal inflammation. *Gut Microbes* **4**, 316–324 (2013).
21. Varela, I. et al. Accelerated ageing in mice deficient in Zmpste24 protease is linked to p53 signalling activation. *Nature* **437**, 564–568 (2005).
22. Rothschild, D. et al. Environment dominates over host genetics in shaping human gut microbiota. *Nature* **555**, 210–215 (2018).
23. Lloyd-Price, J. et al. Strains, functions and dynamics in the expanded Human Microbiome Project. *Nature* **550**, 61–66 (2017).
24. Goodrich, J. K. et al. Human genetics shape the gut microbiome. *Cell* **159**, 789–799 (2014).
25. Gopalakrishnan, V. et al. Gut microbiome modulates response to anti-PD-1 immunotherapy in melanoma patients. *Science* **359**, 97–103 (2018).
26. Routy, B. et al. Gut microbiome influences efficacy of PD-1-based immunotherapy against epithelial tumors. *Science* **359**, 91–97 (2018).
27. Kalabis, J., Rosenberg, I. & Podolsky, D. K. Vangl1 protein acts as a downstream effector of intestinal trefoil factor (ITF)/TFF3 signaling and regulates wound healing of intestinal epithelium. *J. Biol. Chem.* **281**, 6434–6441 (2006).
28. Barcena, C. et al. Methionine restriction extends lifespan in progeroid mice and alters lipid and bile acid metabolism. *Cell Rep.* **24**, 2392–2403 (2018).
29. Ridaura, V. K. et al. Gut microbiota from twins discordant for obesity modulate metabolism in mice. *Science* **341**, 1241214 (2013).
30. Cox, L. M. et al. Altering the intestinal microbiota during a critical developmental window has lasting metabolic consequences. *Cell* **158**, 705–721 (2014).
31. Vrieze, A. et al. Transfer of intestinal microbiota from lean donors increases insulin sensitivity in individuals with metabolic syndrome. *Gastroenterology* **143**, 913–916 (2012).
32. Wang, Y. et al. Fecal microbiota transplantation for refractory immune checkpoint inhibitor-associated colitis. *Nat. Med.* **24**, 1804–1808 (2018).
33. van Nood, E. et al. Duodenal infusion of donor feces for recurrent *Clostridium difficile*. *N. Engl. J. Med.* **368**, 407–415 (2013).
34. Bodogai, M. et al. Commensal bacteria contribute to insulin resistance in aging by activating innate B1a cells. *Sci. Transl. Med.* **10**, eaat4271 (2018).
35. Weingarden, A. R. et al. Microbiota transplantation restores normal fecal bile acid composition in recurrent *Clostridium difficile* infection. *Am. J. Physiol. Gastrointest. Liver Physiol.* **306**, G310–G319 (2014).
36. Buffie, C. G. et al. Precision microbiome reconstitution restores bile acid mediated resistance to *Clostridium difficile*. *Nature* **517**, 205–208 (2015).
37. Zarrinpar, A. et al. Antibiotic-induced microbiome depletion alters metabolic homeostasis by affecting gut signaling and colonic metabolism. *Nat. Commun.* **9**, 2872 (2018).
38. de Aguiar Vallim, T. Q., Tarling, E. J. & Edwards, P. A. Pleiotropic roles of bile acids in metabolism. *Cell Metab.* **17**, 657–669 (2013).
39. Pierre, J. F. et al. Activation of bile acid signaling improves metabolic phenotypes in high-fat diet-induced obese mice. *Am. J. Physiol. Gastrointest. Liver Physiol.* **311**, G286–G304 (2016).
40. Postler, T. S. & Ghosh, S. Understanding the holobiont: how microbial metabolites affect human health and shape the immune system. *Cell Metab.* **26**, 110–130 (2017).

Acknowledgements

The authors thank M. Stamsnijder and the Progeria Family Circle, and all the participants that have kindly engaged in our study. The authors also thank G. Velasco, Y. Español, A.R. Folgueras, X.M. Caravia, J.M. Fraile, I. Varela, M. Mittelbrunn and K. Iribarren for helpful comments and advice; R. Feijoo, A. Moyano, D.A. Puente, S.A. Miranda, M.S. Pitiot, V. García de la Fuente and M.C. Muñiz for excellent technical assistance; M. Gueimonde and C.G. de los Reyes-Gavilán (IPLA-CSIC) for providing *A. muciniphila*; C. Mayolas for help with logistic organization. The authors acknowledge generous support by J.I. Cabrera. A.M.N. is a recipient of a FPI predoctoral contract and N.S. is supported by a Juan de la Cierva postdoctoral contract, both granted by Ministerio de Economia y Competividad (MINECO). A.L.'s research on aging is funded by Fondo de Investigaciones Sanitarias and Fondos FEDER (PI15/00558). The metabolomics platform is supported by H2020 European Union project OncoBiome. G.K. is supported by Ligue contre le Cancer (équipe labellisée); Agence National de la Recherche (ANR) – Projets blancs; ANR under the frame of E-Rare-2, the ERA-Net for Research on Rare Diseases; Association pour la recherche sur le cancer (ARC); Cancéropôle Ile-de-France; Chancelerie des universités de Paris (Legs Poix), Fondation pour la Recherche Médicale (FRM); a donation by Elior; European Research Area Network on Cardiovascular Diseases (ERA-CVD, MINOTAUR); Gustave Roussy Odyssea; the European Union Horizon 2020 Project Oncobiome; Fondation Carrefour; Institut National du Cancer (INCa); Inserm (HTE); Institut Universitaire de France; LeDucq Foundation; the LabEx Immuno-Oncology; the RHU Torino Lumière; the Seerave Foundation; the SIRIC Stratified Oncology Cell DNA Repair and Tumor Immune Elimination (SOCRATE); the SIRIC Cancer Research and Personalized Medicine (CARPEM). The Instituto Universitario de Oncología is supported by Fundación Bancaria Caja de Ahorros de Asturias. J.M.P.F. is supported by Ministerio de Economía y Competitividad-FEDER and Gobierno del Principado de Asturias. C.L.-O. is supported by grants from the European Research Council (DeAge, ERC Advanced Grant), Ministerio de Economía y Competitividad-FEDER, Instituto de Salud Carlos III (RTICC) and Progeria Research Foundation.

Author contributions

C.B., J.M.P.F., P.M.Q. and C.L.-O. conceived and designed the experiments. R.V.-M., P.M.Q. and C.B. performed bioinformatics analysis and results interpretation. C.B., P.M., C.G., F.R. and P.M.Q. performed experiments and analyzed data. M.T.F.-G. performed histopathological analysis. N.S. and A.M.N. performed the culturing and bacterial solutions of *A. muciniphila*. N.G. and A.L. organized and carried out pickup of human centenarian samples. S.D., N.B., F.A. and G.K. performed LC-MS-based metabolomics. C.B., J.M.P.F., P.M.Q. and C.L.-O. wrote the manuscript. A.L. and G.K. assisted with manuscript editing and all authors revised the manuscript and provided input.

Competing interests

G.K. is one of the scientific co-founders of everImmune.

Additional information

Extended data is available for this paper at https://doi.org/10.1038/s41591-019-0504-5.

Supplementary information is available for this paper at https://doi.org/10.1038/s41591-019-0504-5.

Reprints and permissions information is available at www.nature.com/reprints.

Correspondence and requests for materials should be addressed to P.M.Q. or C.L.-O.

Peer review information: Michael Basson and Randy Levinson were the primary editors on this Article and managed its editorial process and peer review in collaboration with the rest of the editorial team.

Publisher's note: Springer Nature remains neutral with regard to jurisdictional claims in published maps and institutional affiliations.

Methods

Mouse models. Both *Lmna*$^{G609G/G609G}$ and *Zmpste24*$^{-/-}$ mice were generated by crossing *Lmna*$^{G609G/+}$ and *Zmpste24*$^{+/-}$ mice and genotyped in our laboratory as previously described[16,21]. All mice used in this study had a C57BL/6N background. Mice were caged separately by sex and transplantation group and checked daily for water and food availability, as well as for good physical condition. Mice were housed in cages with solid floors, sawdust and nests. Every day, mice in all groups were given pellets of food previously softened in water for 1–2 h to facilitate the feeding of progeroid mice. All components of the cages, including food, had been autoclaved previously. For glucose determination, blood samples were obtained from the tail vein and measured with an Accu-Chek glucometer (Roche Diagnostics). Body temperature was measured by rectal probe (Acorn Temp TC Thermocouple Thermometer, Fisher Scientific). Transplantation experiments in progeroid mice began at ~6 to 10 weeks of age. In the *Lmna*$^{G609G/G609G}$ survival experiments, 11 mice were analyzed in control (7 males and 4 females), transplanted with WT (5 males and 6 females) and transplanted with *Lmna*$^{G609G/G609G}$ groups (5 males and 6 females), whereas 8 mice (3 males and 5 females) were analyzed in the empty transplant group. *Zmpste24*$^{-/-}$ transplantation experiments were performed with 7 females per group. In the WT transplantation experiments, 14 animals per group were used (7 males and 7 females). In the WT and *Lmna*$^{G609G/G609G}$ validation experiment, 8 mice (4 males and 4 females) were used in each group of transplanted mice, and pooled samples from 12 WT (6 males and 6 females) and 15 *Lmna*$^{G609G/G609G}$ mice (8 males and 7 females) were used as donors. Survival curves were analyzed with the log-rank (Mantel–Cox) test. Maximum survival was analyzed by Fisher's exact test at the 80th percentile[41]. All animal experiments were approved by the Committee for Animal Experimentation of the Universidad de Oviedo (Spain) and performed in accordance with the European and Spanish legislative and regulatory guidelines (European convention ETS 1 2 3, on the use and protection of vertebrate mammals in experimentation and for other scientific purposes, and Spanish Law 6/2013, and R.D. 53/2013 on the protection and use of animals in scientific research), making every effort to minimize mouse discomfort.

Human samples. We obtained samples from four HGPS families and one NGPS family that include individuals affected with progeria and their healthy siblings. Additionally, we collected samples from a Spanish cohort composed of 17 centenarians, independently of their health status, and 14 healthy ethnically matched adults, aged 30 to 50 years and with no history of any major disease. Research involving humans was approved by the Ethical Committee of Regional Clinical Research of the Principality of Asturias, project no.105/16. All participants read and signed an informed consent.

Preparation of 16S DNA for metagenome profiling. Mouse feces were collected for 4 h and immediately kept at −80 °C until DNA extraction. For human studies, samples were picked and stored at −20 °C in OmniGene Gut kits (ref. OMR-200, DNA Genotek, Ora Sure Techonologies). In all cases (mice and human samples), DNA was extracted using a PowerSoil DNA Isolation kit (MO BIO Laboratories, Quiagen N.V.). DNA quality and quantification were assessed with a Qubit fluorometer (Thermo Fisher Scientific). Libraries were prepared following the 16S Metagenomic Sequencing Library Preparation protocol from Illumina. Briefly, the region V3–V4 from 16S rRNA was amplified using primers 341F/805R to which Illumina Sequencing adapters and dual-index barcodes of the Nextera XT kit were added (fwd 5′-TCGTCGGCAGCGTCAGATGTGTATAAG AGACAGCCTACGGGNGGCWGCAG-3′ and rev 5′-GTCTCGTGGGCTCGG AGA TGTGTATAAGAGACAGGACTACHVGGGTATCTAATCC-3′). Sequencing was performed in a MiSeq platform (IMEGEN) using a 2 × 300 bp-end protocol.

Metagenome profiling. Raw paired-end reads were processed with QIIME 2 (version 2018.6.0). Sequence quality controls were performed with DADA2 (qiime dada2 denoise-paired, with a number of expected errors higher than 6): reads were filtered, trimmed, denoised, dereplicated, forward and reverse sequences were merged and chimeras were removed. Taxonomy was assigned using a pre-trained Naïve Bayes classifier, with a trimmed version of Greengenes 13_8 99% operational taxonomic units (OTUs), which includes the V3–V4 regions, bounded by the 341F/805R primer pair. For the *Lmna*$^{G609G/G609G}$ model, we obtained 3,071,354 paired-end reads of 300 nucleotides each, with 1,084 OTUs identified after quality filtering (Extended Data Fig. 1a), and for *Zmpste24*$^{-/-}$ model, we obtained 1,149,187 paired-end reads of 300 nucleotides each, with 882 OTUs identified after quality filtering (Extended Data Fig. 3a). Four-month-old C57BL/6N WT mice in experiments from Fig. 1 were used as controls for both *Lmna*$^{G609G/G609G}$ and *Zmpste24*$^{-/-}$ mice. For human samples in progeria patients, we obtained 1,709,578 paired-end reads of 300 nucleotides each, with 691 OTUs identified after quality filtering (Extended Data Fig. 4a), whereas for centenarians and healthy controls we obtained 6,196,891 paired-end reads of 300 nucleotides each, with 1,761 OTUs identified after quality filtering (Extended Data Fig. 5a). For validating FMT experiments, eight mice per group and condition were used, obtaining 8,761,200 paired-end reads of 300 nucleotides each, with 18,402 OTUs identified after quality filtering. Alpha-diversity and statistical data were calculated based on different metrics (shannon, chao1). Beta-diversity was measured using Bray–Curtis dissimilarity and the Jaccard similarity index (braycurtis, jaccard). Samples were hierarchical-clustered with the Unweighted Pair Group Method with Arithmetic Mean (UPGMA) method and using different beta-diversity metrics (braycurtis, jaccard). Differences in bacteria abundance were calculated using LEfSe[42]. Metagenome functional content prediction was performed using PICRUSt[43] and HUMAnN2 (v0.11.1)[44] and analyzed with LEfSe.

Microbiota transplants. Before transplantation, mice were treated for three consecutive days with 200 µl of an antibiotic cocktail (with each daily dose being administered by oral gavage after a 6 h fast) that contained 1 g l^{-1} ampicillin, 0.5 g l^{-1} neomycin, 0.5 g l^{-1} vancomycin and 1 g l^{-1} metronidazole. Thereafter, mice were given 100 µl of the microbiota suspension twice a week for two weeks, starting the first day after the antibiotic cycle. After this two-week period, mice received the microbiota suspension once a week until natural death or sacrifice. For the microbiota suspension preparation, 2–5 fresh feces pellets (80–100 mg) were resuspended with a vortex in 600 µl of reduced PBS (PBS with 0.5 g l^{-1} cysteine and 0.2 g l^{-1} Na_2S). After resuspension, tubes containing the feces in reduced PBS were centrifuged at 2,500 r.p.m. (500*g*) for 1 min to remove insolubilized material, and 100 µl of supernatant was administered to the mice by oral gavage. Mice in the empty transplant group received the same antibiotics treatment and were transplanted only with reduced PBS.

Calorimetry measurements. Metabolic parameters (oxygen consumption, carbon dioxide production and total energy expenditure) were obtained using a comprehensive lab animal monitoring system (Oxymax CLAMS, Columbus Instruments) and analyzed following the manufacturer's instructions. Mice were monitored for 48 h; the first 24 h were discarded in the analysis (considered as acclimation period).

***A. muciniphila* culture and oral supplementation.** Cultures of the strain *A. muciniphila* CIP107961 grown for 24 h in GAM medium (Nissui Pharmaceutical Co.) supplemented with 0.25% (wt/vol) L-cysteine (Sigma Chemical Co.) (GAMc) in anaerobic conditions were used to inoculate (2% vol/vol) fresh pre-reduced GAMc broth, which was incubated for 24 h. Afterwards, cultures were washed with PBS and concentrated in anaerobic PBS that included 25% (vol/vol) glycerol to a concentration of about 1 × 10^{10} c.f.u. ml^{-1} under strict anaerobic conditions and stored at −80 °C until use. To test the viability of glycerol stocks, serial dilutions in PBS were made and deep-plated on agar-GAMc. Plates were incubated under anaerobic conditions for 5 days to determine the *Akkermansia* counts (c.f.u. ml^{-1}). Before administration by oral gavage, the glycerol stocks were thawed under anaerobic conditions and diluted with anaerobic PBS to a final concentration of 2 × 10^8 viable c.f.u. per 0.1 ml. *Lmna*$^{G609G/G609G}$ mice were treated by oral gavage with 100 µl of either *Akkermansia* suspension (AKK group, $n = 9$) or anaerobic PBS (control group, $n = 12$) three days a week beginning at 12 weeks of age and until decease.

qPCR. For RNA expression analysis, total RNA from ~30 mg of frozen ileon samples was extracted using Trizol (Life Technologies) and resuspended in nuclease-free water (Life Technologies). A 1–2 µg sample of total RNA was used for reverse transcription using the QuantiTect Reverse Transcription kit (Qiagen NV). cDNA (10× diluted) was used for qPCR using Power SYBR Green PCR Master Mix (Life Technologies) and real-time PCR (7300 HT, Applied Biosystems). Gene expression was normalized to GAPDH expression. For bacterial quantification, DNA from mouse feces was extracted as described above. A 1– 4 ng sample of DNA was used for qPCR reactions using specific primers to amplify bacterial 16S rDNA. Bacterial abundance was assessed by normalizing with the abundance of total bacteria in feces using the conserved eubacterial 16S rDNA primer pair UniF340/UniR514. Results are presented as relative quantification using RQ value ($RQ = 2^{-\Delta\Delta Ct}$). Primer sets for qPCR analyses are shown in Supplementary Table 4.

Metabolomic analysis. Before sacrifice for sample collection, mice were starved overnight and thereafter allowed to eat for 4 h. 30 mg of ileum content for each condition was first weighted and solubilized in 1 ml polypropylene Precellys lysis tubes, with 1 ml of cold lysate buffer (MeOH/water/chloroform, 9/1/1, −20 °C). After being vortexed for 10 min, samples were centrifuged (10 min at 15,000*g*, 4 °C), and the upper phase was collected and split into two parts: the first 270 µl used for gas chromatography coupled to mass spectrometry (GC-MS) and 250 µl used for ultra-high pressure liquid chromatography coupled to mass spectrometry (UHPLC-MS). For GC-MS measurements, 150 µl from the aliquot was transferred to a glass tube and evaporated. Then, 50 µl of methoxyamine (20 mg ml^{-1} in pyridine) was added to dried extracts and samples were stored at room temperature in the dark for 16 h. The next day, 80 µl of *N*-methyl-*N*-(trimethylsilyl)trifluoroacetamide (MSTFA) was added and final derivatization was carried out at 40 °C over 30 min. Samples were then transferred in vials and directly injected into the GC-MS apparatus. For LC-MS measurements, the collected supernatant was evaporated in microcentrifuge tubes at 40 °C in a pneumatically assisted concentrator (Techne DB3, Techne). Dried extracts were solubilized with 450 µl of MilliQ water and aliquoted in three microcentrifuge tubes (100 µl) for each LC method and one microcentrifuge tube for safety. Aliquots were

transferred to LC vials and injected into LC-MS or kept at −80 °C until injection. A daily qualification of the instrumentation was set up with automatic tune and calibration processes. These qualifications were completed with double injections of standards mixes, at the beginning and at the end of the run, as for a blank extracted sample to control the background impurities. Mixtures were adapted for each chromatographic method. After the extraction, fractions of each biological sample were pooled to create a quality control (QC) sample, used to passivate the column before the analysis with the proper biological matrix. This QC sample was reinjected into each batch to monitor and correct analytical bias. Analytical methods and data processing were performed as previously described[45]. Results are presented as the normalized area of the MS picks in $\log_2$ scale using arbitrary units. Normalization was performed by correcting the area of the MS picks across the batches using the QC pooled samples and by centering their values around the mean of the QC areas. Standard reagents (acetonitrile, methanol, chloroform, acetic acid and dibutylamine acetate concentrate) were acquired from Sigma Aldrich. Differentially expressed metabolites in each condition were identified using the moderate *t*-statistic implemented in the R/Bioconductor package limma[46], using sex as a covariate. Metabolites with a nominal $P < 0.05$ and q-value of <0.25 were selected for metabolic set enrichment analysis using a one-sided Fisher's exact test against all metabolites annotated in each KEGG pathway. Metabolomic results are provided in Supplementary Table 5.

Histological analysis. Kidneys and intestines were fixed in 4% paraformaldehyde in PBS and stored in 50% ethanol. Fixed tissues were embedded in paraffin by standard procedures. Blocks were sectioned (5 µm) and stained with hematoxylin and eosin and Masson trichrome (H&E, MT, kidney) and periodic acid Schiff-alcian blue (PAS-AB, intestine). Renal perivascular fibrosis was analyzed/graded from 0 to 4, by using a histology damage score (0, no lesion; 1, focal lesion; 2, multifocal mild lesion; 3, multifocal moderate lesion; 4, diffuse, moderate or severe damage). Five fields were scored from each slide.

Statistical analysis. The number of mice allocated per group was based on previous experiments and their distribution was randomized, as indicated in each figure legend. Comparisons between two groups following a normal distribution were performed using a two-tailed Student's *t*-test, while one-factor ANOVA was used for comparisons of three or more groups. Unless specified in the figure legends, adjusted *P* values were obtained using Tukey's correction. For non-parametric distributions, the Wilcoxon rank-sum and Kruskal–Wallis test (the latter followed by the Dunnett post hoc test) were performed for comparisons between two groups or three or more groups, respectively. Survival analysis was performed using the Kaplan–Meier method and statistical differences were analyzed with the log-rank (Mantel–Cox) test (GraphPad Prism 6.0 and survival R package). Body weight curves were analyzed using a linear-mixed effect model (lme4 R package). The hazard ratio was calculated using a Cox proportional hazards regression model (survival R package). Sample sizes for lifespan experiments were chosen with a power of 80%, based on our previous studies[16,28,47]. Maximal survival was calculated using Fisher's test at the 80th percentile. Plots were generated with GraphPad Prism 6.0 and RStudio (using ggplot2 R package) and edited with Illustrator CC (21.0.0). Statistical analysis was performed using RStudio and GraphPad Prism 6.0. Exact *P* values are indicated in each figure.

Reporting Summary. Further information on research design is available in the Nature Research Reporting Summary linked to this Article.

Data availability

Sequence data supporting these findings have been deposited in EGA (https://ega-archive.org/) under accession number EGAS00001003656. Metabolomics data are provided in Supplementary Table 5. Any additional data generated and analyzed in this study are available from the corresponding authors upon reasonable request.

References

41. Wang, C., Li, Q., Redden, D. T., Weindruch, R. & Allison, D. B. Statistical methods for testing effects on 'maximum lifespan'. *Mech. Ageing Dev.* **125**, 629–632 (2004).
42. Segata, N. et al. Metagenomic biomarker discovery and explanation. *Genome Biol.* **12**, R60 (2011).
43. Langille, M. G. et al. Predictive functional profiling of microbial communities using 16S rRNA marker gene sequences. *Nat. Biotechnol.* **31**, 814–821 (2013).
44. Abubucker, S. et al. Metabolic reconstruction for metagenomic data and its application to the human microbiome. *PLoS Comput. Biol.* **8**, e1002358 (2012).
45. Enot, D. P. et al. Metabolomic analyses reveal that anti-aging metabolites are depleted by palmitate but increased by oleate in vivo. *Cell Cycle* **14**, 2399–2407 (2015).
46. Ritchie, M. E. et al. limma powers differential expression analyses for RNA-sequencing and microarray studies. *Nucleic Acids Res.* **43**, e47 (2015).
47. Osorio, F. G. et al. Nuclear lamina defects cause ATM-dependent NF-κB activation and link accelerated aging to a systemic inflammatory response. *Genes Dev.* **26**, 2311–2324 (2012).

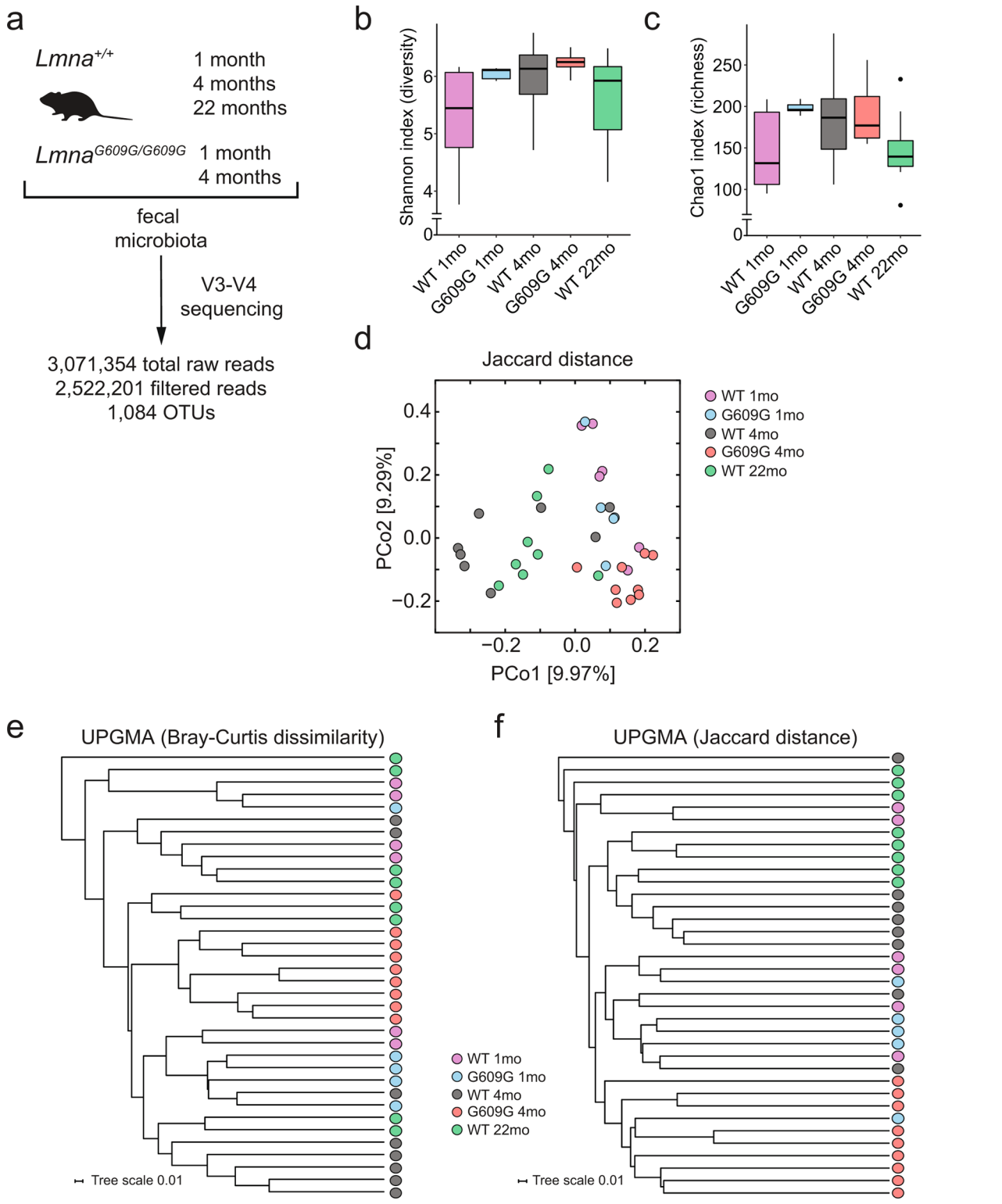

Extended Data Fig. 1 | Biodiversity in wild-type (WT) and *Lmna*$^{G609G/G609G}$ mice at different ages. a, Scheme representing the microbiome profiling experiment in *Lmna*$^{G609G/G609G}$ mice. **b**,**c**, Comparison of alpha-diversity of gut microbiota among all groups of mice using Shannon's index (diversity) (**b**) and the Chao1 index (richness) (**c**). Analyses were performed using Kruskal–Wallis test (Supplementary Table 1). In the box plots, upper and lower hinges correspond to the first and third quartiles, the center line represents the median, whiskers indicate the highest and lowest values that are within 1.5 × IQR and data beyond the end of the whiskers are outliers and plotted as points. **d**, Principal coordinates analysis (PCoA) of beta-diversity using the Jaccard distance metric among samples of the five groups analyzed ($P < 0.001$; PERMANOVA) (Supplementary Table 1). **e**,**f**, UPGMA trees representing the beta-diversity analysis of all groups analyzed using the Bray–Curtis dissimilarity (**e**) and the Jaccard distance metrics (**f**). For **a**–**e**, WT 1mo, $n = 6$; G609G 1mo, $n = 5$; WT 4mo, $n = 8$; G609G 4mo, $n = 9$; WT 22mo, $n = 8$.

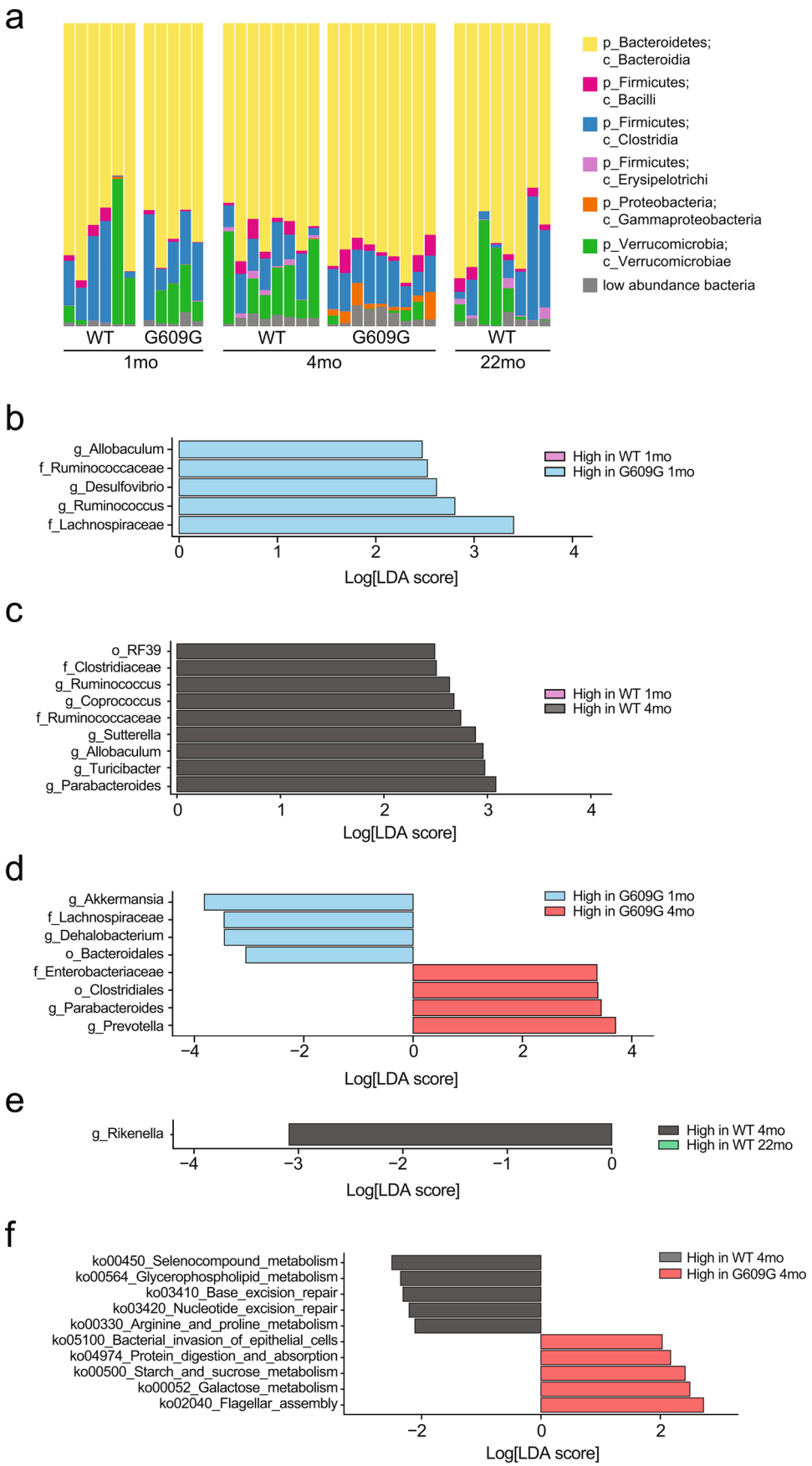

Extended Data Fig. 2 | see figure caption on next page.

Extended Data Fig. 2 | Statistically significant differences in the gut microbiome of *Lmna*$^{G609G/G609G}$ versus wild-type (WT) mice at different ages. a, Total relative abundance of prevalent microbiota at the class level in the five groups studied: 1-month-old WT ($n = 6$), 1-month-old *Lmna*$^{G609G/G609G}$ ($n = 5$), 4-month-old WT ($n = 8$), 4-month-old *Lmna*$^{G609G/G609G}$ ($n = 9$) and 22-month-old WT ($n = 8$), showing data for individual mice. The low-abundance bacteria group includes all bacterial classes with less than 0.5% of total abundance. **b**, Results of LEfSe analysis showing bacteria that were significantly different in abundance in progeroid (blue, $n = 5$) versus WT (violet, $n = 6$) mice at 1 month of age. **c**, Results of LEfSe analysis showing bacteria that were significantly different in abundance between WT mice at 1 (violet, $n = 6$) and 4 (grey, $n = 8$) months of age. **d**, Results of LEfSe analysis showing bacteria that were significantly different in abundance between progeroid mice at 1 (blue, $n = 5$) and 4 (red, $n = 9$) months of age. **e**, Results of LEfSe analysis showing bacteria that were significantly different in abundance between WT mice at 4 (grey, $n = 8$) and 22 (green, $n = 8$) months of age. **f**, Results of LEfSe analysis of PICRUSt-HUMAnN2, showing the top five KEGG pathways (based on *P* value) significantly upregulated in WT and G609G at 4 months (Supplementary Table 3). p, phylum; c, class; o, order; f, family; g, genus. For **a**–**f**, analyses were performed with WT 1mo, $n = 6$; G609G 1mo, $n = 5$; WT 4mo, $n = 8$; G609G 4mo, $n = 9$; WT 22mo, $n = 8$.

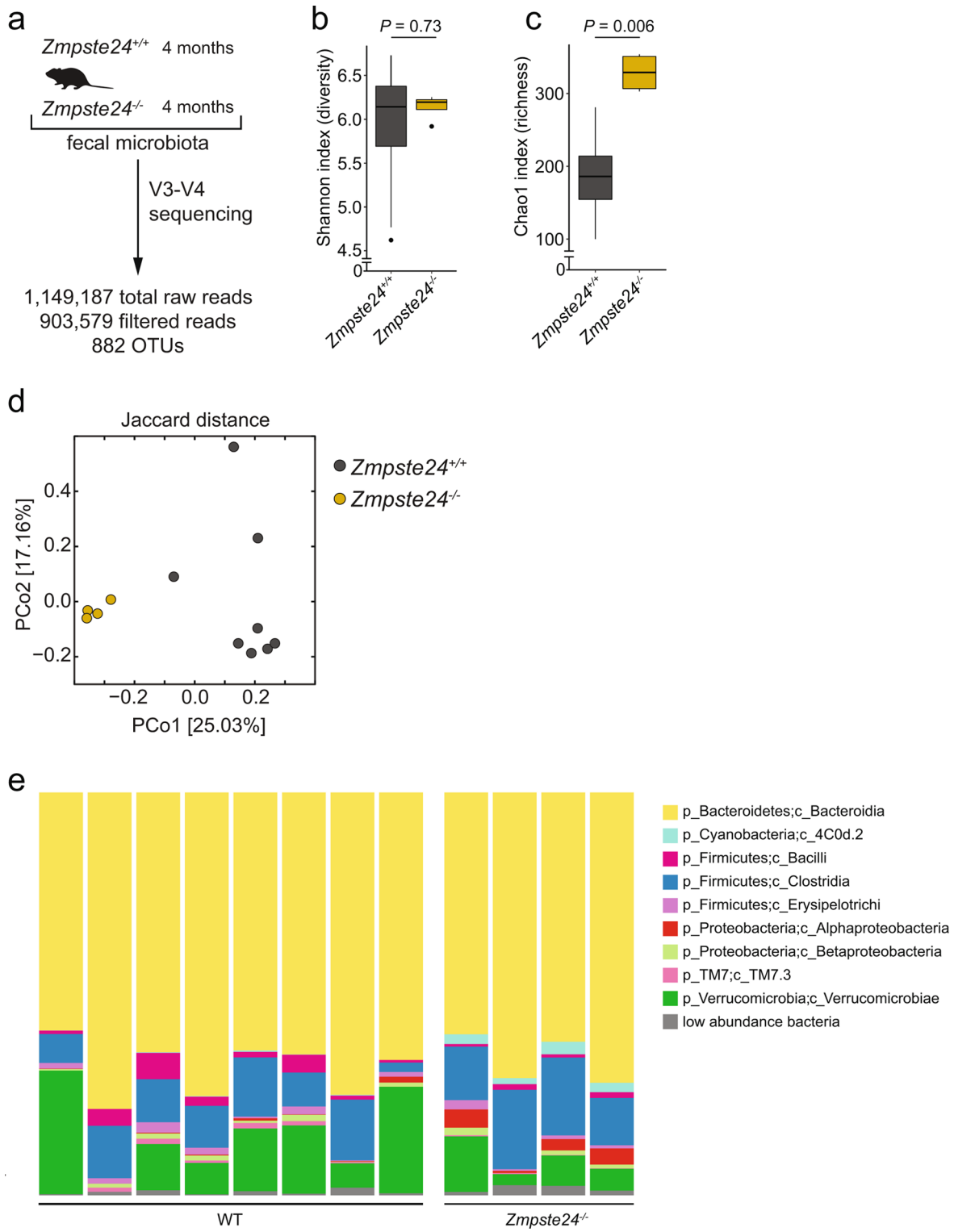

Extended Data Fig. 3 | Gut microbiome alteration in progeroid *Zmpste24*$^{-/-}$ mice. a, Scheme representing the microbiome profiling experiment in *Zmpste24*$^{-/-}$ mice. **b**,**c**, Comparison of alpha-diversity of gut microbiota between WT and *Zmpste24*$^{-/-}$ mice using Shannon's index (diversity) (**b**) and the Chao1 index (richness) (**c**). Analyses were performed using the Kruskal–Wallis test (Supplementary Table 1). In the box plots, upper and lower hinges correspond to the first and third quartiles, the center line represents the median, whiskers expand to the highest and lower values that are within 1.5 × IQR and data beyond the end of the whiskers are outliers and plotted as points. **d**, PCoA of beta-diversity using the Jaccard distance metric between WT and *Zmpste24*$^{-/-}$ mice ($P < 0.002$; PERMANOVA). **e**, Total relative abundance of prevalent microbiota at the class level in *Zmpste24*$^{-/-}$ and WT mice showing results from individual mice. The low abundance bacteria group includes all bacterial classes with less than 0.5% of total abundance. p, phylum; c, class. For **a**–**e**, analyses were performed with WT ($n = 8$) and *Zmpste24*$^{-/-}$ ($n = 4$) mice.

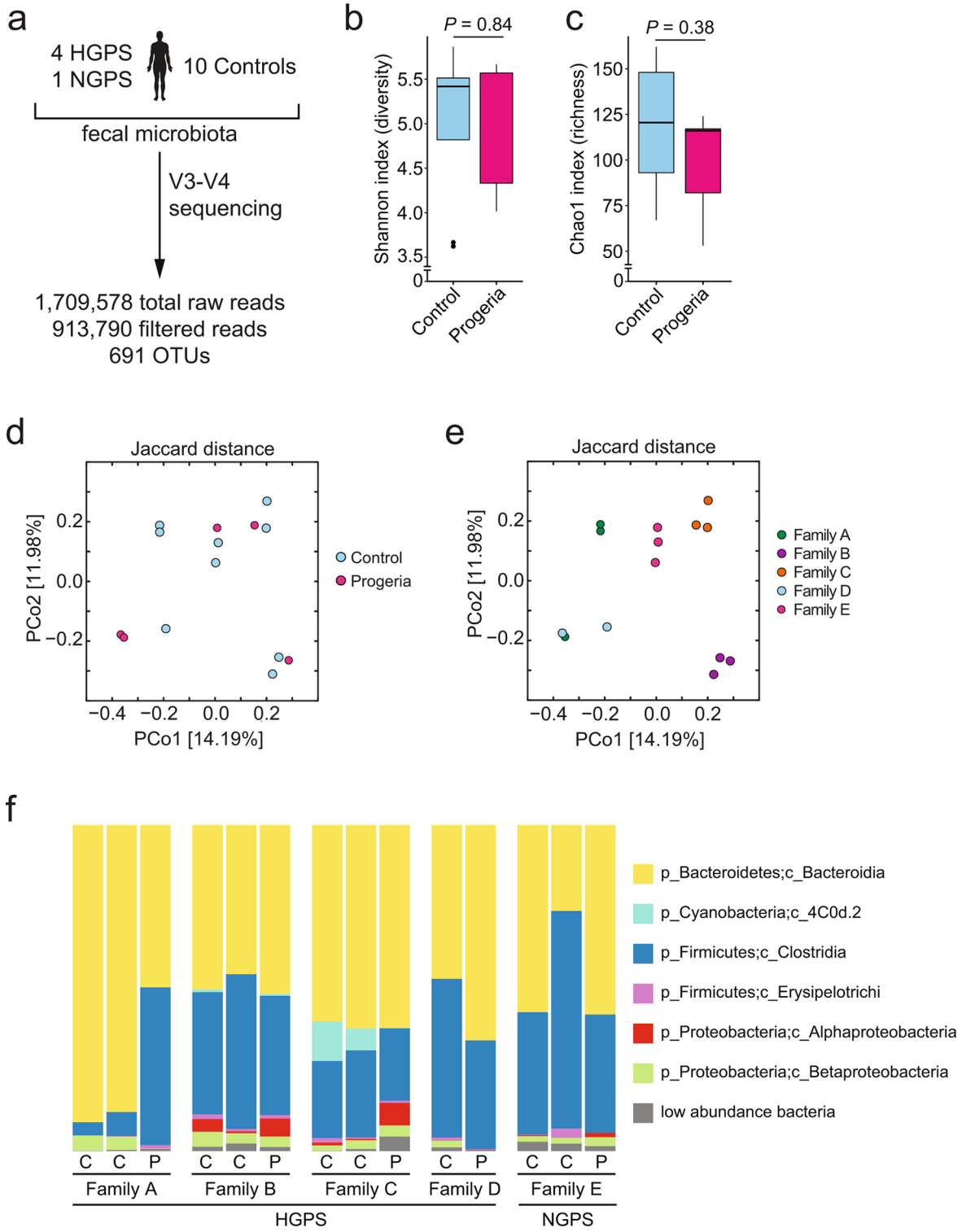

Extended Data Fig. 4 | Gut microbiome alteration in human progeria samples. a, Scheme representing the microbiome profiling experiment in Hutchinson–Gilford (HGPS) and Néstor–Guillermo (NGPS) progeria syndromes. **b**,**c**, Comparison of alpha-diversity of gut microbiota using the Shannon's index (diversity) (**b**) and the Chao1 index (richness) (**c**) between progeria patients and healthy siblings. Analyses were performed using the Kruskal–Wallis test (Supplementary Table 1). In the box plots, upper and lower hinges correspond to the first and third quartiles, the center line represents the median, whiskers indicate the highest and lowest values that are within 1.5 × IQR and data beyond the end of the whiskers are outliers and plotted as points. **d**,**e**, PCoA of beta-diversity using the Jaccard distances metric among samples analyzed by health status ($P = 0.75$, PERMANOVA) (**d**) and by family ($P = 0.001$, PERMANOVA) (**e**) (Supplementary Table 1). **f**, Total relative abundance of prevalent microbiota at the class level in progeria patients and their corresponding healthy relatives, grouped by family and disease condition. The low-abundance bacteria group includes all bacterial classes with less than 0.5% of total abundance. p, phylum; c, class. For **a**–**f**, analyses were performed on family A, $n = 3$ individuals; family B, $n = 3$ individuals; family C, $n = 3$ individuals; family D, $n = 2$ individuals; family E, n = 3 individuals; control (C), $n = 9$ individuals, progeria (P), $n = 5$ individuals.

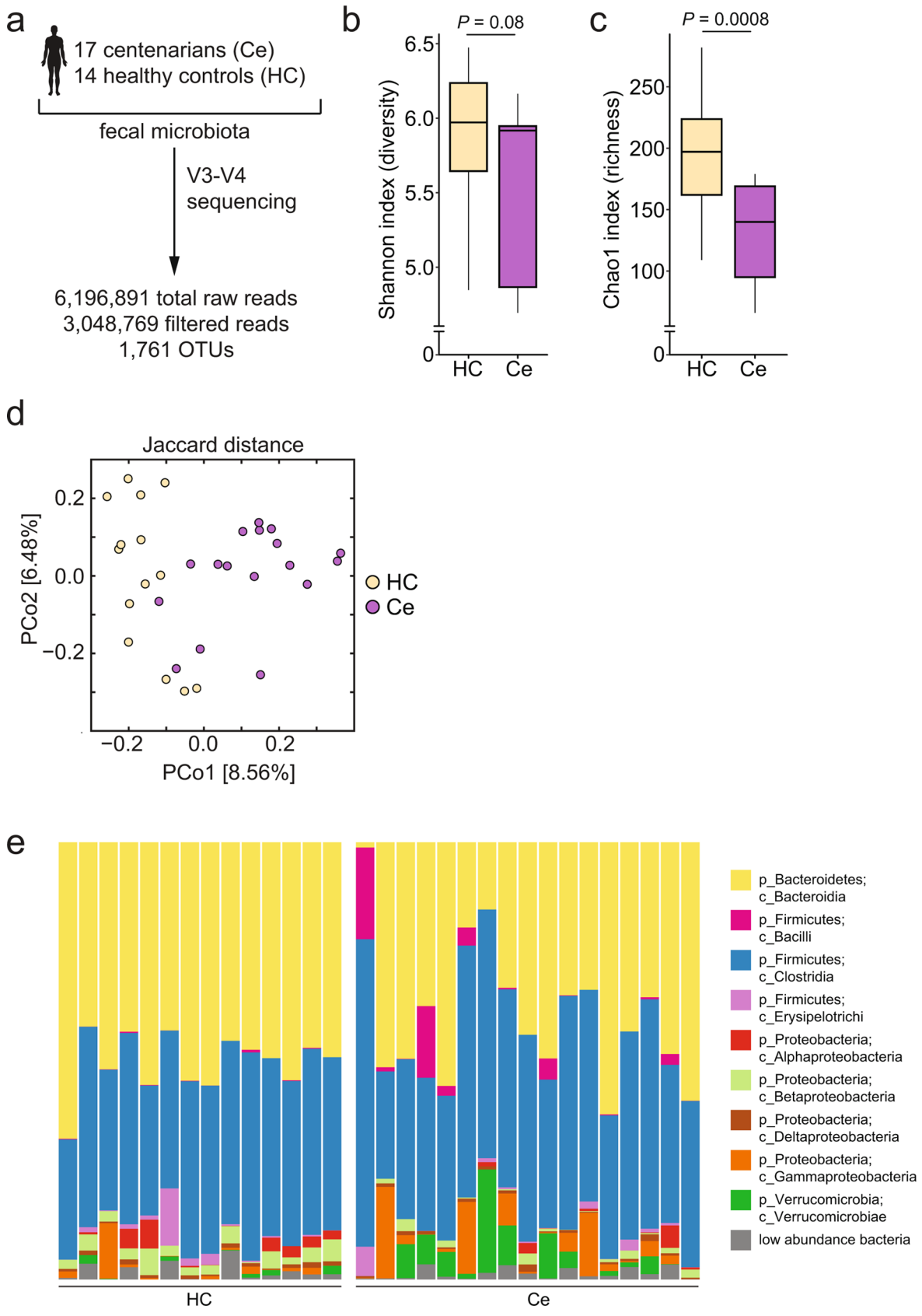

Extended Data Fig. 5 | see figure caption on next page.

Extended Data Fig. 5 | Gut microbiome alteration in human samples from centenarians and healthy controls (adults aged 30–50 years). a, Scheme representing the microbiome profiling experiment of centenarians and healthy controls. **b**,**c**, Comparison of alpha-diversity using Shannon's index (diversity; $P = 0.08$) (**b**) and the Chao1 index (richness; $P = 0.00079$) (**c**) in centenarians compared to healthy controls. Analyses were performed with the Kruskal–Wallis test (Supplementary Table 1). In the box plots, upper and lower hinges correspond to the first and third quartiles, the center line represents the median, whiskers indicate the highest and lowest values that are within 1.5 × IQR and data beyond the end of the whiskers are outliers and plotted as points. **d**, PCoA of beta-diversity using the Jaccard distance metric between centenarians (Ce) and healthy controls (HC) ($P < 0.001$; PERMANOVA). **e**, Total relative abundance of prevalent microbiota at the class level in healthy controls (HC) and centenarians (Ce) showing data for each individual. The low-abundance bacteria group includes all bacterial classes with less than 0.5% of total abundance. p, phylum; c, class. For **a**–**e**, analyses were performed on centenarians (Ce), $n = 17$ individuals, and healthy adult controls (HC), $n = 14$ individuals.

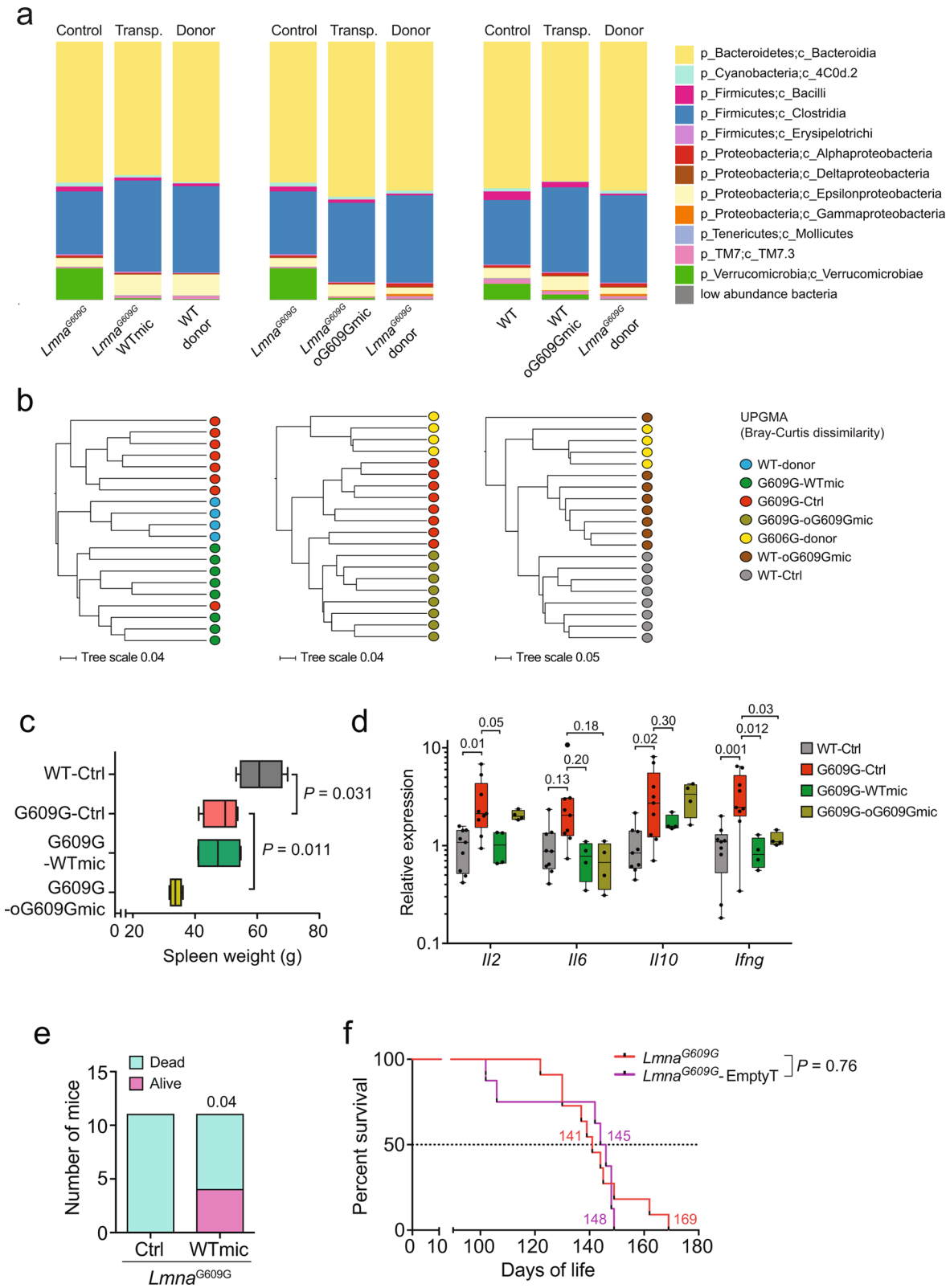

Extended Data Fig. 6 | see figure caption on next page.

Extended Data Fig. 6 | *Lmna*$^{G609G/G609G}$ mice transplanted with wild-type (WT) gut microbiota show an improved healthspan and lifespan. a, Average relative abundance of prevalent microbiota at the class level in the FMT experiments, comparing age-matched controls and transplanted mice ($n = 8$, 4 males and 4 females, in all groups) and donor mice ($n = 4$, pooled samples from male and female mice). The low-abundance bacteria group includes all bacterial classes representing less than 0.1% of the total. Transplants began at ~6–8 weeks of age and metagenome profiling was analyzed after four rounds of FMT (2 weeks after microbiota depletion). Donor mice, both WT and *Lmna*$^{G609G/G609G}$, were ~18–20 weeks old. p, phylum; c, class. **b**, UPGMA trees representing the beta-diversity analysis of control, transplanted and donor mice in each experimental condition, using Bray–Curtis dissimilarity (Supplementary Table 1). **c**, Comparison of spleen weight between control WT ($n = 4$), *Lmna*$^{G609G/G609G}$ ($n = 4$), *Lmna*$^{G609G/G609G}$ mice transplanted with WT microbiota (G609G-WTmic; $n = 4$) and *Lmna*$^{G609G/G609G}$ mice transplanted with microbiota from older *Lmna*$^{G609G/G609G}$ mice (G609G-oG609Gmic $n = 4$). Analyses were performed with one-way ANOVA with Sidak's multiple comparison test. Exact adjusted *P* values are represented within the plot. **d**, mRNA relative levels (in $\log_{10}$ scale) of inflammatory interleukins in the ileum of WT ($n = 9$), G609G-control ($n = 9$), G609G-WTmic ($n = 4$) and G609G-oG609Gmic ($n = 4$) mice. Differences were analyzed with ANOVA with Sidak's multiple comparisons test relative to G609G-control mice. Exact adjusted *P* values are represented within the plot. For **c** and **d**, in the box plots, upper and lower hinges correspond to the first and third quartiles, the center line represents the median, whiskers indicate the highest and lowest values that are within 1.5 × IQR, and data beyond the end of the whiskers are outliers and plotted as points. **e**, Comparison of the number of mice dead and alive between *Lmna*$^{G609G/G609G}$ (Ctrl; $n = 11$) and *Lmna*$^{G609G/G609G}$ mice transplanted with WT microbiota (WTmic; $n = 11$) at the 80th percentile of the overall survival. Differences were analyzed by one-sized Fisher's exact test ($P = 0.04$). **f**, Percentage survival of *Lmna*$^{G609G/G609G}$ ($n = 11$) and *Lmna*$^{G609G/G609G}$ mice transplanted with buffer (*Lmna*^{G609G}-EmptyT; $n = 8$). Transplants started at ~8–10 weeks of age. Differences were analyzed with the log-rank Mantel–Cox test and BH correction was applied after pairwise comparisons between all experimental groups, including those described in Fig. 3f ($P = 0.76$). Hazard ratio (HR) was calculated using a Cox proportional model (HR of 1.7 [95% confidence interval (CI) 0.64–4.88], $P = 0.27$). Median and maximal survival are indicated in the Kaplan–Meier plot.

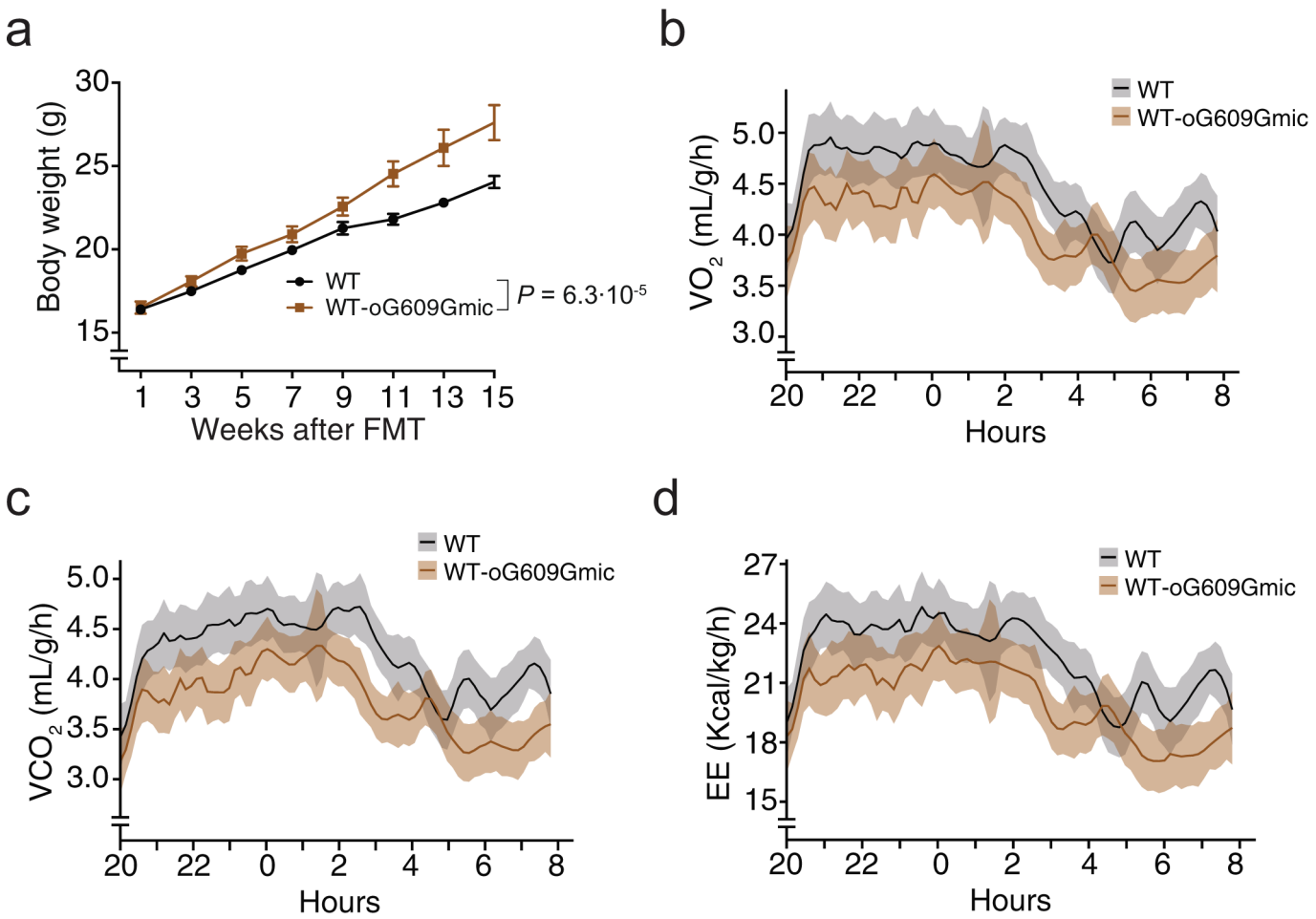

Extended Data Fig. 7 | WT mice transplanted with progeroid microbiota show metabolic alterations. a, Comparison of the body weight between female WT mice transplanted with progeroid microbiota (WT-oG609Gmic; $n = 7$) and female WT controls ($n = 7$) over the indicated time period. Differences of body weight over the time were assessed with a linear mixed model and analyzed with an ANOVA type II Wald χ^2 test ($\chi^2 = 15.98$, d.f. $= 1$, $P = 6.3 \times 10^{-5}$). Data are presented as mean ± s.e.m. **b**–**d**, Metabolic parameters, measured with an Oxymax system, of WT ($n = 14$; 7 males and 7 females) and WT-oG609Gmic ($n = 14$; 7 males and 7 females) mice. Comparison of O_2 consumption (**b**), CO_2 production (**c**) and energy expenditure (**d**) over the indicated period of time. Smoothing curves represent the means of all individuals in each group and shaded areas represent 95% CI.

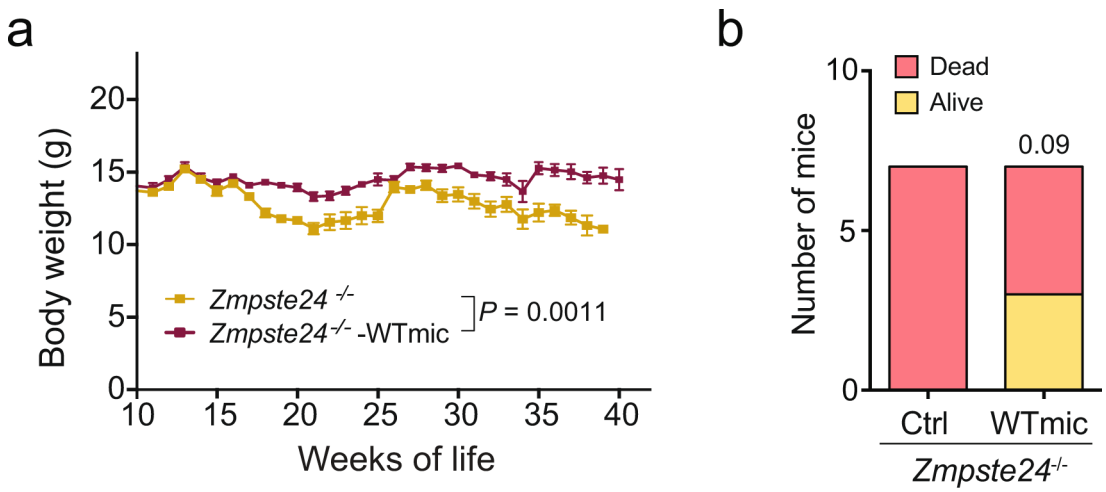

Extended Data Fig. 8 | *Zmpste24*$^{-/-}$ female mice transplanted with wild-type (WT) gut microbiota show an improved phenotype and extended maximal survival. a, Comparison of the body weight between control *Zmpste24*$^{-/-}$ mice ($n = 7$) and *Zmpste24*$^{-/-}$ mice transplanted with WT microbiota (*Zmpste24*$^{-/-}$-WTmic, $n = 7$) over the indicated time period. Differences in body weight over the time were assessed with a linear mixed model and analyzed with an ANOVA type II Wald χ^2 test ($\chi^2 = 10.52$, d.f. = 1, $P = 0.0011$). **b**, Comparison of the number of mice dead and alive between *Zmpste24*$^{-/-}$ (Ctrl; $n = 7$) and *Zmpste24*$^{-/-}$ transplanted with WT microbiota (WTmic; $n = 7$) at the 80th percentile of overall survival. Differences were analyzed by one-sized Fisher's exact test ($P = 0.09$).

nature research

Corresponding author(s): Pedro M. Quirós
Carlos López-Otín

Last updated by author(s): May 7, 2019

Reporting Summary

Nature Research wishes to improve the reproducibility of the work that we publish. This form provides structure for consistency and transparency in reporting. For further information on Nature Research policies, see Authors & Referees and the Editorial Policy Checklist.

Statistics

For all statistical analyses, confirm that the following items are present in the figure legend, table legend, main text, or Methods section.

n/a	Confirmed	
☐	☒	The exact sample size (*n*) for each experimental group/condition, given as a discrete number and unit of measurement
☐	☒	A statement on whether measurements were taken from distinct samples or whether the same sample was measured repeatedly
☐	☒	The statistical test(s) used AND whether they are one- or two-sided *Only common tests should be described solely by name; describe more complex techniques in the Methods section.*
☐	☒	A description of all covariates tested
☐	☒	A description of any assumptions or corrections, such as tests of normality and adjustment for multiple comparisons
☐	☒	A full description of the statistical parameters including central tendency (e.g. means) or other basic estimates (e.g. regression coefficient) AND variation (e.g. standard deviation) or associated estimates of uncertainty (e.g. confidence intervals)
☐	☒	For null hypothesis testing, the test statistic (e.g. *F*, *t*, *r*) with confidence intervals, effect sizes, degrees of freedom and *P* value noted *Give P values as exact values whenever suitable.*
☒	☐	For Bayesian analysis, information on the choice of priors and Markov chain Monte Carlo settings
☒	☐	For hierarchical and complex designs, identification of the appropriate level for tests and full reporting of outcomes
☒	☐	Estimates of effect sizes (e.g. Cohen's *d*, Pearson's *r*), indicating how they were calculated

Our web collection on statistics for biologists contains articles on many of the points above.

Software and code

Policy information about availability of computer code

Data collection	No software was used
Data analysis	For metagenome profiling, QIIME 2 (version 2018.6.0), DADA2, LEfSe, PICRUSt, HUMAnN2 (v0.11.1) were used. For metabolomics analysis R/Bioconductor limma package was used. For survival analysis, R survival package was used. Body weight curves were analyzed using lme4 and car R packages. For graphic representation and statistical analysis, R version 3.1 (base, stats and tidyverse R packages), Rstudio and GraphPad Prism 6.0 were used. Figures were edited with Illustrator CC (21.0.0). All detailed software and packages are described in methods section.

For manuscripts utilizing custom algorithms or software that are central to the research but not yet described in published literature, software must be made available to editors/reviewers. We strongly encourage code deposition in a community repository (e.g. GitHub). See the Nature Research guidelines for submitting code & software for further information.

Data

Policy information about availability of data

All manuscripts must include a data availability statement. This statement should provide the following information, where applicable:

- Accession codes, unique identifiers, or web links for publicly available datasets
- A list of figures that have associated raw data
- A description of any restrictions on data availability

Accession codes are available in the Data availability section included in Methods. Metabolomics data is provided in suplemental figure 5.

Field-specific reporting

Please select the one below that is the best fit for your research. If you are not sure, read the appropriate sections before making your selection.

☒ Life sciences ☐ Behavioural & social sciences ☐ Ecological, evolutionary & environmental sciences

For a reference copy of the document with all sections, see nature.com/documents/nr-reporting-summary-flat.pdf

Life sciences study design

All studies must disclose on these points even when the disclosure is negative.

Sample size	For human studies, no sample-size calculation was performed. Number of samples was selected based on disponibility of the samples, considering the scarcity of centenarians and progeria patients. The results obtained with both centenarian and progeria samples were consistent with those from animal models and prior human studies. In the case of mouse studies, power calculation was used to determine minimum number of mice required for survival and transplantation experiments, chosing a power of 80% based on our previous studies. For the rest of experiments (metagenome profiling, metabolome profiling, qPCR analysis), all samples available from the survival and transplantation experiments were used.
Data exclusions	No data was excluded
Replication	For metagenome analysis of mouse data, sequencing experiments were performed twice, succesfully replicating the results. Results in bacterial taxa modifications between groups that were not replicated in the two different sequencing experiments have not been included in the manuscript. Survival/transplantation studies were also performed in two different experiments, replicating the results. Human sequencing was only performed once due to the scarcity of sample and resources, but the results are in concordance with prior studies.
Randomization	Mice were randomly allocated in the different experimental groups, ensuring only an equal distribution of sexes.
Blinding	Sample collection, library preparation and preliminary analysis of metagenome sequencing and metabolome studies were performed by blinded technicians and computational biologists.

Reporting for specific materials, systems and methods

We require information from authors about some types of materials, experimental systems and methods used in many studies. Here, indicate whether each material, system or method listed is relevant to your study. If you are not sure if a list item applies to your research, read the appropriate section before selecting a response.

Materials & experimental systems

n/a	Involved in the study
☒	☐ Antibodies
☒	☐ Eukaryotic cell lines
☒	☐ Palaeontology
☐	☒ Animals and other organisms
☐	☒ Human research participants
☒	☐ Clinical data

Methods

n/a	Involved in the study
☒	☐ ChIP-seq
☒	☐ Flow cytometry
☒	☐ MRI-based neuroimaging

Animals and other organisms

Policy information about studies involving animals; ARRIVE guidelines recommended for reporting animal research

Laboratory animals	We used C57BL/6N mus musculus, both male and female. Experiments began around 6-8 weeks of age.
Wild animals	The study did not involve wild animals
Field-collected samples	The study did not involve field-collected samples
Ethics oversight	All animal experiments were approved by the Committee for Animal Experimentation of the Universidad de Oviedo (Spain) and performed in accordance with the European and Spanish legislative and regulatory guidelines (European convention ETS 1 2 3, on the use and protection of vertebrate mammals in experimentation and for other scientific purposes, and Spanish Law 6/2013, and R.D. 53/2013 on the protection and use of animals in scientific research)

Note that full information on the approval of the study protocol must also be provided in the manuscript.

Human research participants

Policy information about studies involving human research participants

Population characteristics	Centenarians were all Spanish, of both sexes. No major health conditions were reported. Controls for centenarians were Spanish adults aged 30-50 years, of both sexes and that had not been in a hospital or with any relevant pathological conditions in the previous year. Progeria patients were aged 8-28years, 2 females and 3 males. Families were from Germany, Finland, Belgium and Spain. All molecularly diagnosed with progeria (four Hutchinson-Gilford progeria and one with Nestor-Guillermo progeria). Controls were their healthy siblings.
Recruitment	Centenarians and controls were a Spanish cohort for longevity studies coordinated by A. Lucia. Families with progeria were contacted by Marjet Stamsnijder, coordinator of the Progeria Family Circle, based of their interest in participating in research studies. No bias was applied.
Ethics oversight	Research involving humans was approved by the Ethical Committee of Regional Clinical Research of the Principality of Asturias, project no.105/16. All participants signed an informed consent.

Note that full information on the approval of the study protocol must also be provided in the manuscript.